OPTIMIZATION OF

SPIRAL INDUCTORS AND LC RESONATORS

EXPLOITING SPACE MAPPING TECHNOLOGY

To my parents

OPTIMIZATION OF

SPIRAL INDUCTORS AND LC RESONATORS

EXPLOITING SPACE MAPPING TECHNOLOGY

By

WENHUAN YU, B. Sc. (Eng.)

A Thesis

Submitted to the School of Graduate Studies

in Partial Fulfillment of the Requirements

for the Degree

Master of Applied Science

McMaster University

MASTER OF APPLIED SCIENCE (2006) McMASTER UNIVERSITY
(Electrical and Computer Engineering) Hamilton, Ontario

TITLE: **Optimization of Spiral Inductors and LC Resonators Exploiting Space Mapping Technology**

AUTHOR: Wenhuan Yu
B.Sc. (Eng) (Electrical Engineering, Shanghai Jiaotong University)

SUPERVISOR: J.W. Bandler, Professor Emeritus,
Department of Electrical and Computer Engineering
B.Sc.(Eng), Ph.D., D.Sc.(Eng) (University of London)
D.I.C. (Imperial College)
P.Eng. (Province of Ontario)
C.Eng., FIEE (United Kingdom)
Fellow, IEEE
Fellow, Royal Society of Canada
Fellow, Engineering Institute of Canada
Fellow, Canadian Academy of Engineering

NUMBER OF PAGES: xvi, 100

ABSTRACT

This thesis contributes to the computer-aided design (CAD) of spiral inductors and LC resonators with spiral inductors exploiting full-wave electromagnetic (EM) analysis.

The spiral inductor is widely used in radio frequency integrated circuits (RF ICs), such as low noise amplifiers (LNA) and voltage controlled oscillators (VCO). The design of spiral inductors has a direct influence on the performance of these circuits. Recently proposed optimization methods for spiral inductors are usually based on circuit models, which are computationally efficient but inaccurate compared with full-wave electromagnetic (EM) simulations.

For the first time, we develop an optimization technique for the design of spiral inductors and LC resonators exploiting both the computational efficiency of a (cheap) circuit model and the accuracy of a full-wave EM analysis, based on geometric programming (GP) and space mapping (SM). With the new technique, we can efficiently obtain EM-validated designs with considerable improvement over those obtained with traditional optimization methods.

ABSTRACT

ACKNOWLEDGEMENT

I wish to express my sincere thanks to my supervisor Dr. John W. Bandler, Simulation Optimization Systems Research Laboratory, McMaster University and President, Bandler Corporation, for his constant support and professional advice.

I would like to extend thanks to my colleagues Dr. Qingsha Cheng, Daniel M. Hailu, Dongying Li, Yan Li, Ying Li, Dr. Slawomir Koziel, Dr. Ahmed S. Mohamed and Jiang Zhu, for their suggestions and encouragement. I also thank Dr. James C. Rautio, President, Sonnet Software, Inc., North Syracuse, NY, for making Sonnet ***em*** available for this research.

I wish to acknowledge financial assistance provided by the Department of Electrical and Computer Engineering, McMaster University, through a Teaching Assistantship, Research Assistantship and Scholarship.

Finally, I would like to express my deep gratitude to my parents, who gave me the strength to finish this work, for their continuous care and support.

ACKNOWLEDGEMENT

CONTENTS

CONTENTS

CONTENTS

LIST OF FIGURES

LIST OF FIGURES

LIST OF TABLES

LIST OF TABLES

LIST OF ACRONYMS

ASM	Aggressive Space Mapping
BPF	Bandpass Filter
CAD	Computer-Aided Design
CMOS	Complementary Metal-Oxide Semiconductor
GP	Geometric Programming
GSM	General Space Mapping
IC	Integrated Circuit
ISM	Implicit Space Mapping
LNA	Low Noise Amplifier
MADS	Mesh Adaptive Direct Search
MEMS	Microelectromechanical Systems
OSM	Output Space Mapping
PGS	Patterned Ground Shield
RF	Radio Frequency
SM	Space Mapping
SOC	System-On-a-Chip

LIST OF ACRONYMS

SQP	Sequential Quadratic Programming
VCO	Voltage Controlled Oscillator
WLAN	Wireless Local-Area Network

CHAPTER 1

INTRODUCTION

With the emergence of cellular phone, wireless local-area network (WLAN) and Bluetooth technology, we are standing on the threshold of a new radio frequency epoch. Compared with the old epoch dominated by discrete bipolar transistors and discrete filters, the new epoch is remarkable for the development of radio frequency integrated circuits (RF ICs), especially Si RF ICs, which are cheaper to fabricate and easier to integrate than GaAs ICs. In the new epoch, most of the radio transceiver components, such as low noise amplifiers (LNA), mixers, oscillators and filters will be integrated on one monolithic chip, sometimes with digital baseband circuits as system-on-a-chip (SOC). By doing this, the cost and the difficulty of assembly and tuning are reduced drastically.

The integrated spiral inductor plays an important role in the development of Si RF ICs. As pointed out in [1], the first published integrated CMOS RF amplifier was hidden in a paper on fabricating a suspended spiral inductor on silicon [2] in 1993. This is because a source-degenerating inductor has to be used to tune the transistor capacitance to obtain gain at RF frequency. This inductor

has to be built on-chip so that the parasitic capacitance coming with the off-chip inductor does not ruin the performance of the amplifier.

The spiral inductor has a great influence on the performance of many RF circuits. The obvious example is the LC tank, in which the quality factor Q of the spiral inductor determines the bandwidth and the resonance impedance of the LC tank. Another example is the bandpass filter (BPF) built with inductors and capacitors, in which the quality factor of the spiral inductor determines the insertion loss [3]. In low noise amplifiers (LNA), the quality factor of the spiral inductor determines the figure of merit (FoM), which is the measure of the overall performance of the LNA [3]. In voltage controlled oscillators (VCO), high-Q spiral inductors reduce both DC power consumption and phase noise [3].

The spiral inductor was once thought to be impractical to be built on heavily doped silicon due to large substrate losses. This situation changed since 1990s, when the first spiral inductor built on silicon was reported [4]. In 1993, a 100-nH suspended on-chip spiral inductor was fabricated by removing the silicon substrate under the spiral inductor [2]. In 1995, a multi-layer spiral inductor was proposed and fabricated [5][6]. In 1996, high-resistivity silicon was used to reduce the substrate loss [7]. In 1998, a patterned ground shield between the spiral inductor and silicon substrate was introduced to separate the electric field of the spiral inductor from the substrate [8]. By the late 1990s, the effort to suspend the spiral inductor from the substrate using MEMS (Microelectromechanical

Systems) technology [9]-[11] gradually developed into a new field by its own: RF MEMS [12].

Following the success in fabrication, intensive research has been conducted in the modeling of spiral inductors on silicon. One approach is to use a compact circuit model. In [13] and [14], a physically based circuit model is proposed. In [15] and [16], two empirical circuit models are proposed. In [17], the circuit model is constructed by calculating the effect of each segment of the spiral inductor and the interconnection between them. The other approach is to solve Maxwell's equations, using electromagnetic simulators, such as ASITIC [18], Sonnet ***em*** [19] and Agilent Momentum [20].

At the same time, a lot of work has been done in the synthesis and optimization of spiral inductors on silicon. Most of these works are based on circuit models. In [21], an analytical design procedure based on the physical model is presented. In [22] and [23], geometric programming (GP) formulation of the spiral inductor optimization is proposed, based on the model presented in [16]. In [24] and [25], sequential quadratic programming (SQP) and an optimization method called mesh adaptive direct search (MADS) are used to optimize the spiral inductor, both are based on circuit models. Although these methods are very efficient, the results they give depend on the quality of the circuit model they use. It is likely that the design does not meet the specification when validated by EM simulators or measurements.

Thus direct optimization based on more accurate EM simulators is highly desirable. Unfortunately, the task is extremely time-consuming, if not impossible, with current computational power. To address this problem, Bandler *et al*. introduced space mapping (SM) technology [26]-[33] in 1994 to incorporate the computational efficiency of cheap circuit models and the accuracy of expensive EM simulations. Space mapping algorithms perform optimization on a cheap circuit model and use EM simulations to calibrate the circuit model. Reviews of recent developments of space mapping technology are given in [28] and [29].

The purpose of this thesis is to present an optimization method for the design of spiral inductors and LC resonators using the space mapping technique. With this method, EM-validated designs can be obtained in minutes or hours, instead of days and weeks.

In Chapter 2, a review of the recent works on the modeling and optimization of spiral inductors is given. For modeling, we focus on a physically based circuit model [14] and an empirical circuit model compatible with geometric programming [16]. For optimization, we focus on the geometric programming formulation of the spiral inductor optimization [22].

In Chapter 3, we review the development of space mapping technology, focusing on the implicit space mapping (ISM) [30] and the general flow of SM-based optimization [33]. We also propose a modified parameter extraction (PE) scheme.

In Chapter 4, we apply space mapping technology to the optimization of spiral inductors and LC resonators. We simplify the GP formulation of the spiral inductor optimization and improve the GP formulation of the LC resonator optimization, which are introduced into an implicit space mapping design process. Two examples show that EM-validated designs of spiral inductors and LC resonators can be obtained in ten full-wave EM simulations.

The thesis is concluded in Chapter 5 with proposals for future work.

The author's original contributions to this thesis are:

(1) Applying space mapping technology to the optimization of spiral inductors and LC resonators.

(2) Proposing a simplified GP formulation for the spiral inductor optimization that can be integrated into an implicit space mapping framework.

(3) Improving the geometric programming formulation for LC resonator optimization.

(4) Developing a modified parameter extraction method which can be partially turned into convex optimization problems.

REFERENCES

[1] A.A. Abidi, "RF CMOS comes of age," *IEEE J. Solid-State Circuits*, vol. 39, no. 4, pp. 549-561, Apr. 2004.

[2] J.Y.-C. Chang, A.A. Abidi and M. Gaitan, "Large suspended inductors on silicon and their use in a 2-μm CMOS RF amplifier," *IEEE Electron Device Lett.*, vol. 14, no. 5, pp. 246-248, May 1993.

[3] J.N. Burghartz, D.C. Edelstein, M. Soyuer, H.A. Ainspan and K.A. Jenkins, "RF circuit design aspects of spiral inductors on silicon," *IEEE J. Solid-State Circuits*, vol. 33, no. 12, pp. 2028-2034, Dec. 1998.

[4] N.M. Nguyen and R.G. Meyer, "Si IC-compatible inductors and LC passive filters," *IEEE J. Solid-State Circuits*, vol. 25, no. 4, pp. 1028-1031, Aug. 1990.

[5] R.B. Merrill, T.W. Lee, H. You, R. Rasmussen and L.A. Moberly, "Optimization of high Q integrated inductors for multi-level metal CMOS," *IEDM 1995*, pp. 38.7.1-38.7.3.

[6] J.N. Burghartz, M. Soyuer and K. Jenkins, "Microwave inductors and capacitors in standard multilevel interconnect silicon technology," *IEEE Trans. Microwave Theory Tech*, vol. 44, no. 1, pp. 100-103, Jan. 1996.

[7] K.B. Ashby, I.A. Koullias, W.C. Finley, J.J. Bastek and S. Moinian, "High Q inductors for wireless applications in a complementary silicon bipolar process," *IEEE J. Solid-State Circuits*, vol. 31, no. 1, pp. 4-9, Jan. 1996.

[8] C. Yue and S. Wong, "On-chip spiral inductors with patterned ground shields for Si-based RF IC's," *IEEE J. Solid State Circuits*, vol. 33, no. 5, pp. 743-752, May 1998.

[9] J.Y. Park and M.G. Allen, "High Q spiral-type microinductors on silicon substrates," *IEEE Trans. Magn.*, vol. 35, no. 5, pp. 3544-3546, Sep. 1999.

[10] H. Jiang, Y. Wang, J.L. Andrew and N.C. Tien, "On-chip spiral inductors suspended over deep copper-lined cavities," *IEEE Trans. Microwave Theory Tech.,* vol. 48, no. 12, pp. 2415-2423, Dec. 2000.

[11] J.B. Yoon, Y.S. Choi, B.I. Kim, Y. Eo and E. Yoon, "CMOS-compatible surface-micromachined suspended-spiral inductors for multi-GHz silicon

RF ICs," *IEEE Electron Device Lett.*, vol. 23, no. 10, pp. 591-593, Oct. 2002.

[12] G.M. Rebeiz, *RF MEMS: Theory, Design and Technology*, New York: Wiley, 2003.

[13] C.P. Yue, C. Ryu, J. Lau, T.H. Lee and S.S. Wong, "A physical model for planar spiral inductors on silicon," *Techn. Dig. IEDM*, pp. 155-158, 1996.

[14] C.P. Yue and S.S. Wong, "Physical modeling of spiral inductors on silicon," *IEEE Trans. on Electron Devices*, vol. 47, no. 3, pp. 560-568, Mar. 2000.

[15] K.B. Ashby, I.A. Koullias, W.C. Finley, J.J. Bastek and S. Moinian, "High Q inductors for wireless applications in a complementary silicon bipolar process," *IEEE J. Solid-State Circuits*, vol. 31, no. 1, pp. 4-9, Jan. 1996.

[16] S.S. Mohan, M. Hershenson, S.P. Boyd and T.H. Lee, "Simple accurate expressions for planar spiral inductances," *IEEE J. Solid-State Circuits*, vol. 34, no. 10, pp. 1419-1424, Oct. 1999.

[17] J.R. Long and M.A. Copeland, "The modeling, characterization, and design of monolithic inductors for silicon RF IC's," *IEEE J. Solid-State Circuits*, vol. 32, no. 3, pp. 357-369, Mar. 1997.

[18] A. Niknejad, ASITIC: Analysis and Simulation of Spiral Inductors and Transformers for ICs, Univ. California, Berkeley, [Online]. Available: http://rfic.eecs.berkeley.edu/~niknejad/asitic.html.

[19] ***em***, Sonnet Software, Inc. 100 Elwood Davis Road, North Syracuse, NY 13212, USA.

[20] Agilent Momentum, Agilent Technologies, 1400 Fountaingrove Parkway, Santa Rosa, CA 95403-1799, USA.

[21] C.-Y. Lee, T.-S. Chen, J.D.-S. Deng and C.-H. Kao, "A simple systematic spiral inductor design with perfected Q improvement for CMOS RFIC application," *IEEE Trans. Microwave Theory Tech.*, vol. 53, no. 2, pp. 523-528, Feb. 2005.

[22] M. Hershenson, S.S. Mohan, S.P. Boyd and T.H. Lee, "Optimization of inductor circuits via geometric programming," *Proc. 36th Design Automation Conf.*, pp. 994-998, Jun. 1999.

[23] G. Stojanovic and L. Zivanov, "Comparison of optimal design of different spiral inductors," *24th Int. Conf. Microelectronics*, vol. 2, pp. 613-616, May 2004.

[24] Y. Zhan and S.S. Sapatnekar, "Optimization of integrated spiral inductors using sequential quadratic programming," *2004 Design, Automation and Test in Europe Conf. Exhibition*, vol. 1, pp. 622-627, Feb. 2004.

[25] A. Nieuwoudt and Y. Massoud, "Multi-level approach for integrated spiral inductor optimization," *Proc. 42nd Design Automation Conf.*, pp. 648-651, Jun. 2005.

[26] J.W. Bandler, R.M. Biernacki, S.H. Chen, P.A. Grobelny and R.H. Hemmers, "Space mapping technique for electromagnetic optimization," *IEEE Trans. Microwave Theory Tech.*, vol. 42, no. 12, pp. 2536-2544, Dec. 1994.

[27] J.W. Bandler, R.M. Biernacki, S.H. Chen, R.H. Hemmers and K. Madsen, "Electromagnetic optimization exploiting aggressive space mapping," *IEEE Trans. Microwave Theory Tech.*, vol. 43, no. 12, pp. 2874-2882, Dec. 1995.

[28] J.W. Bandler, Q.S. Cheng, S.A. Dakroury, A.S. Mohamed, M.H. Bakr, K. Madsen and J. Søndergaard, "Trends in space mapping technology for engineering optimization," *3rd Annual McMaster Optimization Conference: Theory and Applications, MOPTA03*, Hamilton, ON, Aug. 2003.

[29] J.W. Bandler, Q. Cheng, S.A. Dakroury, A.S. Mohamed, M.H. Bakr, K. Madsen and J. Søndergaard, "Space mapping: the state of the art," *IEEE Trans. Microwave Theory and Tech.*, vol. 52, no. 1, pp. 337-361, Jan. 2004.

[30] J.W. Bandler, Q.S. Cheng, N.K. Nikolova and M.A. Ismail, "Implicit space mapping optimization exploiting preassigned parameters," *IEEE Trans. Microwave Theory Tech.*, vol. 52, no. 1, pp. 378-385, Jan. 2004.

[31] J.W. Bandler, Q.S. Cheng, D. Gebre-Mariam, K. Madsen, F. Pedersen and J. Søndergaard, "EM-based surrogate modeling and design exploiting implicit, frequency and output space mappings," *IEEE MTT-S Int. Microwave Symp. Dig.*, Philadelphia, PA, 2003, pp. 1003-1006.

[32] J.W. Bandler, D.M. Hailu, K. Madsen and F. Pedersen, "A space mapping interpolating surrogate algorithm for highly optimized EM-based design of microwavee devices," *IEEE Trans. Microwave Theory and Tech.*, vol. 52, no. 11, pp. 2593-2600, Nov. 2004.

[33] J.W. Bandler, Q.S. Cheng, D.M. Hailu and N.K. Nikolova, "A space-mapping design framework," *IEEE Trans. Microwave Theory Tech.*, vol. 52, no. 11, pp. 2601-2610, Nov. 2004.

CHAPTER 1 INTRODUCTION

CHAPTER 2

RECENT WORK ON THE MODELING AND OPTIMIZATION OF SPIRAL INDUCTORS ON SILICON

2.1 INTRODUCTION

Inductors are components used to store energy in the form of magnetic fields. In RF integrated circuits, inductors of spiral shape are fabricated on metal layers. As an example, the top and sectional view of a square inductor fabricated in a sample CMOS process are shown in Fig. 2.1 and Fig. 2.2. Two metal layers are used: the top layer for the spiral inductor and the lower layer for the underpass (the part shown by the dotted line in Fig. 2.1). The geometry parameters of the spiral inductor are the number of turns n, the width of the metal trace w, the turn spacing s, the inner diameter d_{in} and the outer diameter d_{out}.

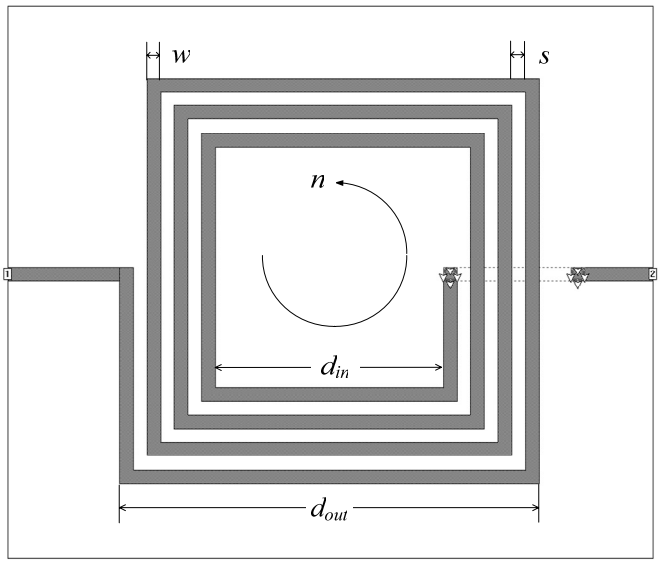

Fig. 2.1 Square spiral inductor (top view) [1].

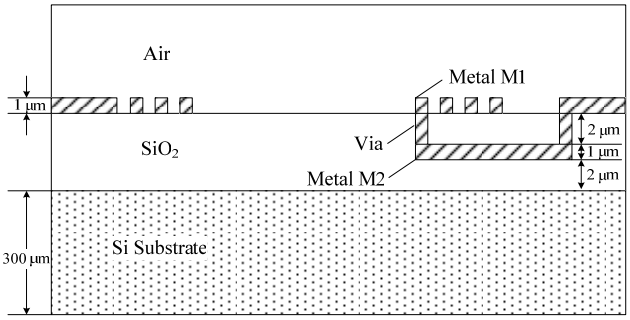

Fig. 2.2 Square spiral inductor (sectional view) [1].

Spiral inductors can be fabricated in other shapes. Fig. 2.3 shows spiral inductors in hexagonal, octagonal and circular shapes. In order to enhance the quality factor, multi-level metal layers are sometimes connected in parallel to fabricate the spiral inductor [3]. For the same purpose, the patterned ground shield (PGS) made with the metal layer between the spiral inductor and the substrate can be used (Fig. 2.4).

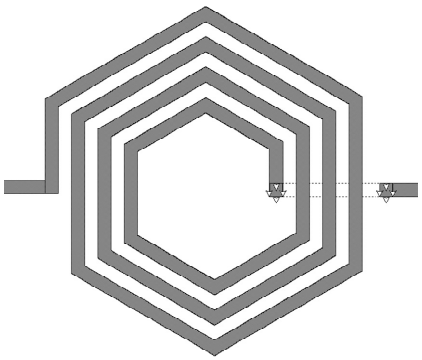

(a)

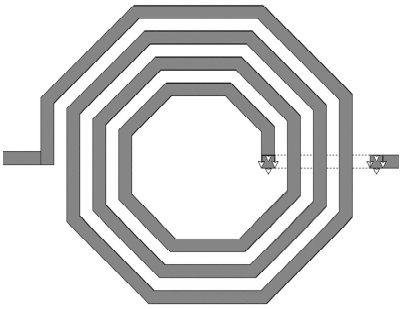

(b)

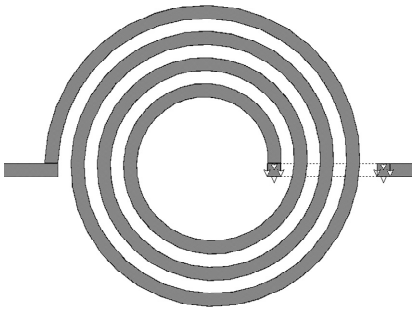

(c)

Fig. 2.3 Spiral inductor: (a) hexagonal, (b) octagonal, and (c) circular.

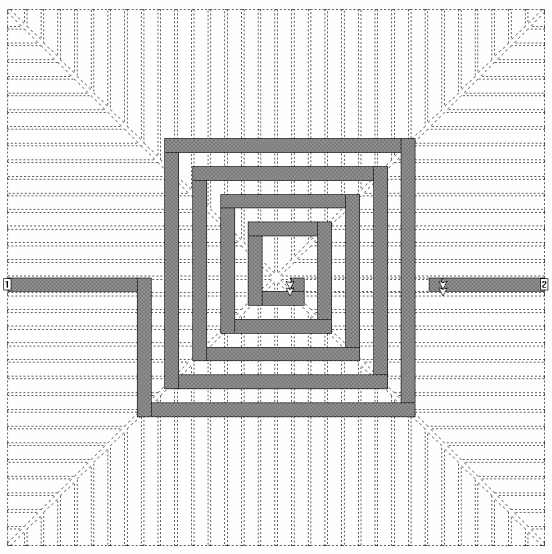

Fig. 2.4 A spiral inductor with the patterned ground shield.

2.2 PHYSICALLY BASED CIRCUIT MODEL

Circuit models have been used since the first paper on spiral inductors on silicon [5], in which a simple circuit model shown in Fig. 2.5 has been proposed.

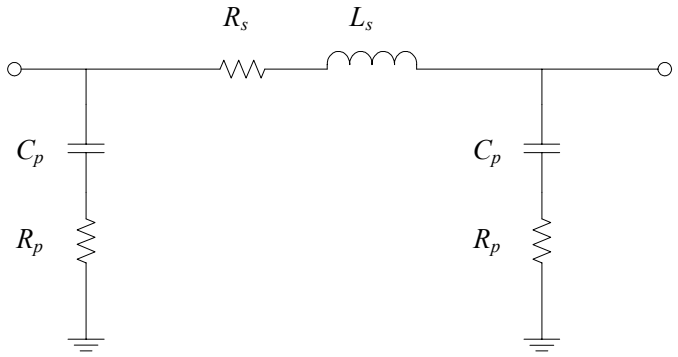

Fig. 2.5 A simple circuit model of the spiral inductor [5].

In this circuit model, the inductor L_s models the inductance of the spiral inductor and the resistor R_s models the resistance of the metal trace. The

capacitor C_p represents the capacitor between the metal and the substrate. The resistor R_p models the conductive Si substrate.

A more widely used model (Fig. 2.6) is proposed in [6]. In this model, C_s is added to represent the direct coupling through the overlap between the spiral and the underpass. The substrate is modeled by three components. The capacitor C_{ox} models the oxide capacitance between the spiral and the substrate. The capacitor C_{si} and the resistor R_{si} represent the capacitance and resistance of silicon substrate.

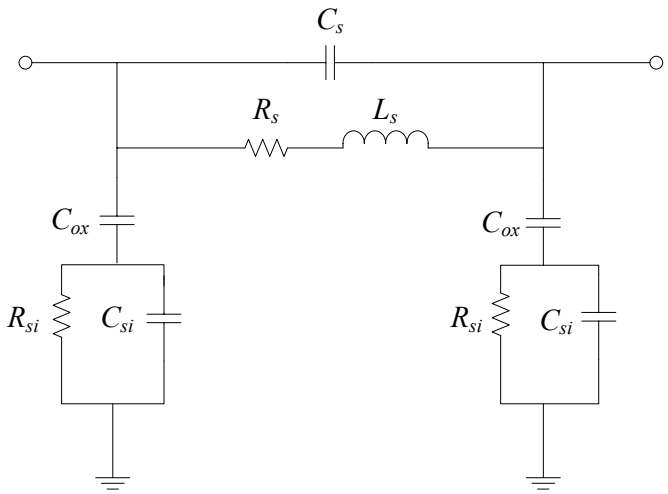

Fig. 2.6 A widely used circuit model of the spiral inductor [6].

In [6] and [7], physically-based equations are proposed to calculate the circuit elements using the geometry parameters of the spiral inductor and technology parameters of the fabrication process. These equations are listed from (2.1) to (2.5)

$$R_s = \frac{l}{\sigma \cdot w \cdot \delta \cdot (1 - e^{-t/\delta})} \tag{2.1}$$

$$C_s = n \cdot w^2 \cdot \frac{\varepsilon_{ox}}{t_{ox\ \text{M1-M2}}} \tag{2.2}$$

$$C_{ox} = \frac{1}{2} \cdot l \cdot w \cdot \frac{\varepsilon_{ox}}{t_{ox}} \tag{2.3}$$

$$C_{si} = \frac{1}{2} \cdot l \cdot w \cdot C_{sub} \tag{2.4}$$

$$R_{si} = \frac{2}{l \cdot w \cdot G_{sub}} \tag{2.5}$$

where σ is the conductivity of the metal layer, l is the total length of the metal trace, δ is the metal skin depth, t is the metal thickness, ε_{ox} is the permittivity of the oxide, $t_{ox\ \text{M1-M2}}$ is the oxide thickness between the spiral inductor and the underpass, t_{ox} is the oxide thickness between the spiral inductor and the substrate, C_{sub} and G_{sub} are the substrate capacitance and conductance per area. The metal skin depth is

$$\delta = \sqrt{\frac{1}{\sigma \cdot \pi \cdot \mu \cdot f}} \tag{2.6}$$

where μ is the permeability and f is the frequency.

2.3 INDUCTANCE CALCULATION

Many methods have been proposed to calculate the inductance L_s and they can be divided into two categories. The first ones are based on the self and mutual inductance calculation for single wires. The second ones are empirical equations.

The basic equations for the first kind of method are summarized in [8]. In particular, the self-inductance of a wire with a rectangular cross-section is [7]

$$L_{self} = 2l \cdot (\ln \frac{2l}{w+t} + 0.5 + \frac{w+t}{3l}) \tag{2.7}$$

where L_{self} is the self inductance in nH, l is the wire length in cm, w is the wire width in cm and t is the wire thickness in cm. This equation only applies when the wire length is greater than approximately twice the cross-section dimension. The mutual inductance between two parallel wires can be expressed as [7]

$$M = 2 \cdot l \cdot Q_m \tag{2.8}$$

where M is the mutual inductance in nH, l is the wire length in cm and Q_m is the mutual inductance parameter [7]

$$Q_m = \ln\left[\frac{l}{GMD} + \sqrt{1+(\frac{l}{GMD})^2}\right] - \sqrt{1+(\frac{GMD}{l})^2} + \frac{GMD}{l}. \tag{2.9}$$

The GMD in (2.9) refers to the geometric mean distance between wires. It is approximately equal to the pitch of the wires (the distance between the central line of the wire). A more precise definition for GMD is [7]

$$\ln GMD = \ln d - \frac{w^2}{12d^2} - \frac{w^4}{60d^4} - \frac{w^6}{168d^6} - \frac{w^8}{360d^8} - \frac{w^{10}}{660d^{10}} - \cdots \quad (2.10)$$

where d is the pitch of the wires and w is the width of the wires.

Based on (2.7) and (2.8), Greenhouse proposed a method to calculate the inductance of the spiral inductor [9]. As shown in Fig. 2.7, the spiral inductor is divided into single wires. The inductance of the spiral inductor is then calculated from the self-inductances and the mutual inductances of these wires. The general equation for this calculation is [9]

$$L_T = L_0 + M_+ - M_- \quad (2.11)$$

where L_T is the total inductance of the spiral inductor, L_0 is the sum of self-inductances, M_+ is the sum of positive mutual inductances (when the current in two parallel wires is in the same direction) and M_- is the sum of negative mutual inductances (when the current in two parallel wires is in the opposite direction).

As an example, the inductance for the spiral inductor in Fig. 2.7 can be calculated as

$$\begin{aligned} L_T = {} & L_1 + L_2 + L_3 + L_4 + L_5 + L_6 + L_7 + L_8 + 2(M_{1,5} + M_{2,6} + M_{3,7} \\ & + M_{4,8}) - 2(M_{1,7} + M_{1,3} + M_{5,7} + M_{5,3} + M_{2,8} + M_{2,4} + M_{6,8} \\ & + M_{6,4}) \end{aligned} \quad (2.12)$$

where L_i is the self-inductance of the wire i and $M_{i,j}$ is the mutual inductance between wire i and wire j.

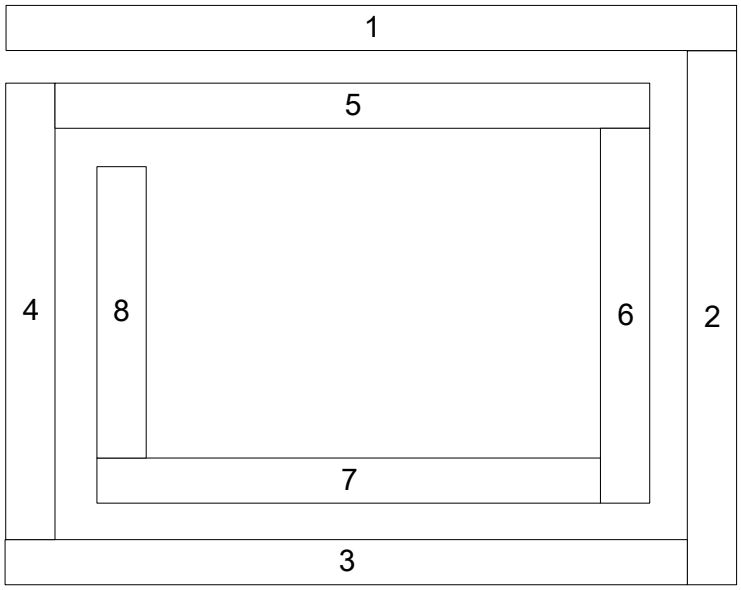

Fig. 2.7 A two-turn spiral inductor [9].

The second kind of method for inductance calculation is empirical equations. One example is the modified Wheeler formula proposed in [2]

$$L_{mw} = K_1 \mu_0 \frac{n^2 d_{avg}}{1 + K_2 \rho} \tag{2.13}$$

where L_{mv} is the inductance calculated by modified Wheeler formula, K_1 and K_2 are coefficients related to the shape of the spiral inductor, n is the number of turns, d_{avg} is the average diameter defined as $d_{avg} = 0.5(d_{in} + d_{out})$, and ρ is the fill ratio defined as $\rho = (d_{out} - d_{in})/(d_{out} + d_{in})$.

Another example is the monomial expression proposed in [2]

$$L_{mon} = \beta d_{out}^{\alpha_1} w^{\alpha_2} d_{avg}^{\alpha_3} n^{\alpha_4} s^{\alpha_5} \tag{2.14}$$

where L_{mon} is the inductance in nH, d_{out} is the outer diameter in μm, w is the metal width in μm, d_{avg} is the average diameter in μm, n is the number of turns and s is

the turn space in μm. The coefficients $\beta, \alpha_1, \alpha_2, \alpha_3, \alpha_4$ and α_5 are extracted through data fitting. These coefficients for spiral inductors of different shapes are found in [2] and listed in Table 2.1. The monomial expression is the basis of the geometric programming formulation of the spiral inductor optimization, which is discussed in Section 2.6.

TABLE 2.1

COEFFICIENTS FOR THE MONOMIAL EXPRESSION OF THE INDUCTANCE [2]

Inductor Shape	β	α_1	α_2	α_3	α_4	α_5
Square	1.62×10^{-3}	-1.21	-0.147	2.40	1.78	-0.030
Hexagonal	1.28×10^{-3}	-1.24	-0.174	2.47	1.77	-0.049
Octagonal	1.33×10^{-3}	-1.21	-0.163	2.43	1.75	-0.049

The inductance can also be calculated from the *Y* parameters (or *Z* parameters) as [11]

$$L_s = -\frac{1}{2\pi f}\,\mathrm{Im}\left(\frac{1}{Y_{12}}\right) \tag{2.15}$$

where f is the frequency. We will use (2.15) to calculate the inductance using the *Y* parameter obtained from an EM simulator.

2.4 QUALITY FACTOR

The fundamental definition of quality factor (Q) of the inductor is [10]

$$Q = 2\pi \frac{\text{energy stored}}{\text{energy loss in one oscillation cycle}}. \tag{2.16}$$

This definition works for both inductors and LC tanks. However, as pointed out in [4], for inductors, the nominator in (2.16) stands for the net magnetic energy, i.e., the difference between peak magnetic energy and peak electric energy stored. This is because for inductors, we are only interested in the magnetic energy stored. The electric energy stored in the parasitic capacitors is harmful and has to be deducted. For LC tanks, the energy stored is the sum of average electric and magnetic energy, or the peak magnetic (electric) energy since the total energy in the LC tank is constant.

In [4], an analytical expression for the quality factor of the spiral inductor is proposed based on the circuit model presented in the same paper (Fig. 2.6). To do this, the circuit model is first transformed into its equivalent circuit with one end connected to the ground (Fig. 2.8). The frequency-dependent components R_p and C_p are calculated as [4]

$$R_p = \frac{1}{\omega^2 C_{ox}^2 R_{si}} + \frac{R_{si}(C_{ox} + C_{si})^2}{C_{ox}^2} \tag{2.17}$$

$$C_p = C_{ox} \cdot \frac{1 + \omega^2 (C_{ox} + C_{si}) C_{si} R_{si}^2}{1 + \omega^2 (C_{ox} + C_{si})^2 R_{si}^2}. \tag{2.18}$$

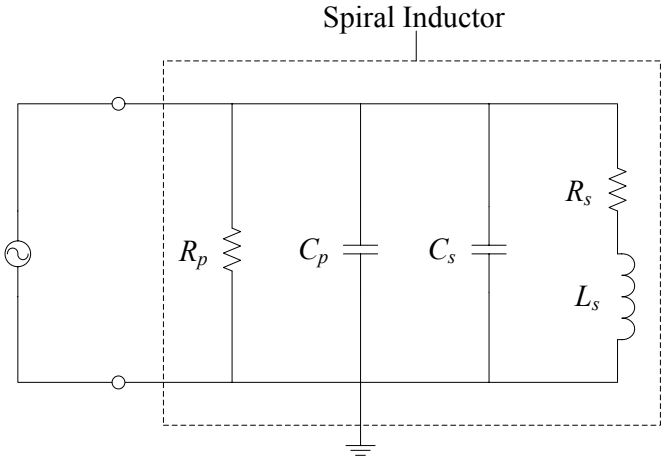

Fig. 2.8 Equivalent circuit model of the spiral inductor with one end connected to the ground [4].

Then we can calculate the peak magnetic energy, the peak electric energy and the energy loss in one oscillation cycle [4]

$$E_{\text{peak magnetic}} = \frac{V_0^2 L_s}{2 \cdot [(\omega L_s)^2 + R_s^2]} \tag{2.19}$$

$$E_{\text{peak electric}} = \frac{V_0^2 (C_s + C_p)}{2} \tag{2.20}$$

$$E_{\text{loss in one oscillation cycle}} = \frac{2\pi}{\omega} \cdot \frac{V_0^2}{2} \cdot \left[\frac{1}{R_p} + \frac{R_s}{(\omega L_s)^2 + R_s^2} \right]. \tag{2.21}$$

According to the definition (2.16), the quality factor can be calculated as

$$\begin{aligned} Q &= 2\pi \cdot \frac{E_{\text{peak magnetic}} - E_{\text{peak electric}}}{E_{\text{loss in one oscillation cycle}}} \\ &= \frac{\omega L_s}{R_s} \cdot \frac{R_p}{R_p + [(\omega L_s / R_s)^2 + 1] R_s} \\ &\quad \cdot \left[1 - \frac{R_s^2 (C_s + C_p)}{L_s} - \omega^2 L_s (C_s + C_p) \right] \end{aligned} \tag{2.22}$$

Based on the same definition, the quality factor can also be calculated from the *Y* parameters (or *Z* parameters) as [11]

$$Q = -\frac{\mathrm{Im}(Y_{11})}{\mathrm{Re}(Y_{11})}. \tag{2.23}$$

We will use (2.23) to calculate the quality factor using the *Y* parameter obtained from an EM simulator.

2.5 SPIRAL INDUCTOR OPTIMIZATION

A typical spiral inductor optimization problem can be expressed as

$$\begin{aligned} &\max\ Q(d_{out}, w, s, n) \\ &s.t.\ L_{s\min} \le L_s(d_{out}, w, s, n) \le L_{s\max} \\ &\quad (2n+1)(s+w) \le d_{out} \\ &\quad d_{out\min} \le d_{out} \le d_{out\max} \\ &\quad w_{\min} \le w \le w_{\max} \\ &\quad s_{\min} \le s \le s_{\max} \\ &\quad n_{\min} \le n \le n_{\max} \end{aligned} \quad . \tag{2.24}$$

We optimize the geometry of the spiral inductor to maximize the quality factor *Q* at the target frequency. The first constraint is used to get the specified inductance. The second constraint is used to ensure that the layout physically exists. The remaining four constraints are for the geometric parameters.

Many optimization methods have been used to solve (2.24), including exhaustive enumeration, sequential quadratic programming (SQP) [12], Mesh-Adaptive Direct Search (MADS) [13] and geometric programming (GP) [14][15].

In the next section, we give a brief review on the GP formulation of the problem, which is integrated into our SM-based optimization algorithm.

2.6 GEOMETRIC PROGRAMMING FORMULATION FOR SPIRAL INDUCTOR OPTIMIZATION [14]

Geometric programming is a special optimization problem that can be converted into a convex optimization problem and solved efficiently. A GP can be written as [14]

$$\begin{aligned} &\min\ f_0(\boldsymbol{x}) \\ &s.t.\ f_i(\boldsymbol{x}) \le 1,\ \ i = 1,2,\ldots,m, \\ &\quad g_i(\boldsymbol{x}) = 1,\ \ i = 1,2,\ldots,p, \\ &\quad x_i > 0,\ \ i = 1,2,\ldots,n, \end{aligned} \tag{2.25}$$

where $f_i(\boldsymbol{x}),\ i = 0,1,\ldots,m,$ are posynomial functions and $g_i(\boldsymbol{x}),\ i = 1,2,\ldots,p,$ are monomial functions. The posynomial function is defined as [14]

$$f(x_1,\ldots,x_n) = \sum_{k=1}^{t} c_k x_1^{\alpha_{1k}} x_2^{\alpha_{2k}} \cdots x_n^{\alpha_{nk}} \tag{2.26}$$

where $c_k > 0,\ k = 1,\ldots,t,$ and $\alpha_{ik} \in R,\ i = 1,\ldots,n,\ k = 1,\ldots,t$. If $t = 1$, $f(\boldsymbol{x})$ is called a monomial function. For example, $f(\boldsymbol{x}) = 0.7 + 0.8x_1x_2 + 0.9x_1^{0.1}x_2^{0.2}$ is a posynomial function and $f(\boldsymbol{x}) = 0.9x_1^{0.1}x_2^{0.2}$ is a monomial function. However, $f(\boldsymbol{x}) = 0.7 + 0.8x_1x_2 - 0.9x_1^{0.1}x_2^{0.2}$ is not a posynomial function because the coefficient of the last term is negative.

GP problems can be solved globally and efficiently by converting the problem into convex optimization problems [16]. By introducing a set of new variables [16]

$$y_i = \log x_i,\ i = 1,\ldots,n, \tag{2.27}$$

we turn the problem (2.25) into its equivalent form [16]

$$\begin{aligned} &\min \ \log f_0(e^{\mathbf{y}}) \\ &s.t. \ \log f_i(e^{\mathbf{y}}) \le 0, \ \ i = 1,2,\ldots,m, \\ &\quad \log g_i(e^{\mathbf{y}}) = 0, \ \ i = 1,2,\ldots,p, \end{aligned} \tag{2.28}$$

where the notation $e^{\mathbf{y}}$ represents a vector in which $(e^{\mathbf{y}})_i = e^{y_i}$. Problem (2.28) is a convex optimization problem [16].

The spiral inductor optimization problem is formulated as a GP problem in [14]. Based on the monomial expression for inductance proposed in [2], the authors expressed all the circuit elements in the circuit model (Fig. 2.6) as monomial functions of the geometry parameters (d_{out}, w, d_{avg}, n and s) [14]

$$L_s = \beta d_{out}^{\alpha_1} w^{\alpha_2} d_{avg}^{\alpha_3} n^{\alpha_4} s^{\alpha_5} \tag{2.29}$$

$$R_s = l/(\sigma w \delta(1 - e^{-t/\delta})) = 4 f(\omega) k_1 d_{avg} n / w \tag{2.30}$$

$$C_{ox} = (\varepsilon_{ox} l w)/(2 t_{ox}) = 4 k_2 d_{avg} n w \tag{2.31}$$

$$C_s = (\varepsilon_{ox} n w^2)/(t_{ox,\text{M1-M2}}) = k_3 n w^2 \tag{2.32}$$

$$C_{si} = (C_{sub} l w)/2 = 4 k_4 d_{avg} n w \tag{2.33}$$

$$R_{si} = 2/(G_{sub} l w) = k_5/(4 d_{avg} n w) \tag{2.34}$$

where L_s is the inductance in nH, d_{out} is the outer diameter in μm, w is the metal width in μm, d_{avg} is the average diameter in μm, n is the number of turns, s is the turn space in μm, k_1 to k_5 are coefficients dependent on technology and $f(\omega)$ is the coefficient dependent on frequency and technology

$$f(\omega) = 1/\left[\sqrt{2/(\omega\mu_0\sigma)}(1-e^{-t/\sqrt{2/(\omega\mu_0\sigma)}})\right]. \tag{2.35}$$

Furthermore, the R_p and C_p in (2.17) and (2.18) can also be expressed as monomial functions of the design parameters [14]

$$R_p = \frac{1}{\omega^2 C_{ox}^2 R_{si}} + \frac{R_{si}(C_{ox}+C_{si})^2}{C_{ox}^2} = k_6/(4d_{avg}nw) \tag{2.36}$$

$$C_p = C_{ox}\cdot\frac{1+\omega^2(C_{ox}+C_{si})C_{si}R_{si}^2}{1+\omega^2(C_{ox}+C_{si})^2 R_{si}^2} = 4k_7 d_{avg} nw\,. \tag{2.37}$$

where k_6 and k_7 are coefficients dependent on technology and frequency.

Unfortunately, as given in (2.22), the objective function (quality factor Q) can not be expressed as a posynomial function of the design parameters. In [14], this problem is solved by introducing a new design variable Q_{min} [14]

$$\begin{aligned}
&\max\ Q_{\min}\\
&s.t.\ \ Q \ge Q_{\min}\\
&\quad L_{s\min} \le L_s \le L_{s\max}\\
&\quad (2n+1)(s+w) \le d_{out}\\
&\quad d_{avg} + n(s+w) \le d_{out}\\
&\quad d_{out\min} \le d_{out} \le d_{out\max}\\
&\quad w_{\min} \le w \le w_{\max}\\
&\quad s_{\min} \le s \le s_{\max}\\
&\quad n_{\min} \le n \le n_{\max}
\end{aligned} \tag{2.38}$$

where the first constraint can be turned into the following posynomial inequality constraint

$$\frac{Q_{\min} R_s}{\omega L_s R_p}\left[R_p + \frac{(\omega L_s)^2}{R_s} + R_s\right] + \frac{R_s^2 (C_s + C_p)}{L_s} + \omega^2 L_s (C_s + C_p) \le 1. \quad (2.39)$$

The design parameters in (2.38) are d_{out}, w, d_{avg}, n and s. Since only four of these design parameters are independent, an equality constraint reflecting the relationship between them has to be added

$$d_{avg} + (n-1)s + nw = d_{out}. \quad (2.40)$$

However, because only equality constraints in monomial form are allowed in the GP, (2.40) is relaxed into the fourth inequality constraint in (2.38). It is pointed out in [14] that this constraint is tight in general cases.

REFERENCES

[1] W. Yu and J.W. Bandler, "Optimization of spiral inductor on silicon using space mapping," *IEEE MTT-S Int. Microwave Symp. Dig.*, San Francisco, CA, Jun. 2006, pp. 1085-1088.

[2] S.S. Mohan, M. Hershenson, S.P. Boyd and T.H. Lee, "Simple accurate expressions for planar spiral inductances," *IEEE J. Solid-State Circuits*, vol. 34, no. 10, pp. 1419-1424, Oct. 1999.

[3] J.N. Burghartz, M. Soyuer and K. Jenkins, "Microwave inductors and capacitors in standard multilevel interconnect silicon technology," *IEEE Trans. Microwave Theory Tech.*, vol. 44, no. 1, pp. 100-103, Jan. 1996.

[4] C. Yue and S. Wong, "On-chip spiral inductors with patterned ground shields for Si-based RF IC's," *IEEE J. Solid State Circuits*, vol. 33, no. 5, pp. 743-752, May 1998.

[5] N.M. Nguyen and R.G. Meyer, "Si IC-compatible inductors and LC passive filters," *IEEE J. Solid-State Circuits*, vol. 25, no. 4, pp. 1028-1031, Aug. 1990.

[6] C.P. Yue, C. Ryu, J. Lau, T.H. Lee and S.S. Wong, "A physical model for planar spiral inductors on silicon," *Techn. Dig. IEDM*, pp. 155-158, 1996.

[7] C.P. Yue and S.S. Wong, "Physical modeling of spiral inductors on silicon," *IEEE Trans. on Electron Devices*, vol. 47, no. 3, pp. 560-568, Mar. 2000.

[8] F.W. Grover, *Inductance Calculations*, New York, NY: Van Nostrand, 1962.

[9] H.M. Greenhouse, "Design of planar rectangular microelectronic inductors," *IEEE Trans. Parts, Hybrids, Pack.*, vol. 10, no. 2, pp. 101-109, Jun. 1974.

[10] H.G. Booker, *Energy in Electromagnetism*, London/New York: Peter Peregrinus (on behalf of the IEE), 1982.

[11] K. Okada, H. Hoshino and H. Onodera, "Modeling and optimization of on-chip spiral inductor in S-parameter domain," *2004 Int. Symp. Circuits and Systems*, vol. 5, pp. 153-156, May 2004.

[12] Y. Zhan and S.S. Sapatnekar, "Optimization of integrated spiral inductors using sequential quadratic programming," *2004 Design, Automation and Test in Europe Conf. Exhibition*, vol. 1, pp. 622-627, Feb. 2004.

[13] A. Nieuwoudt and Y. Massoud, "Multi-level approach for integrated spiral inductor optimization," *Proc. 42nd Design Automation Conf.*, pp. 648-651, Jun. 2005.

[14] M. Hershenson, S.S. Mohan, S.P. Boyd and T.H. Lee, "Optimization of inductor circuits via geometric programming," *Proc. 36th Design Automation Conf.*, pp. 994-998, Jun. 1999.

[15] G. Stojanovic and L. Zivanov, "Comparison of optimal design of different spiral inductors," *24th Int. Conf. Microelectronics*, vol. 2, pp. 613-616, May 2004.

[16] S. Boyd and L. Vandenberghe, *Convex Optimization*, Cambridge University Press, Cambridge, 2004.

CHAPTER 2 RECENT WORK … OF SPIRAL INDUCTORS ON SILICON

CHAPTER 3

SPACE MAPPING TECHNOLOGY

3.1 INTRODUCTION

With the development of CAD technology, optimization has become a widely used technique in RF and microwave circuit design. A typical design problem is to choose the design parameters (e.g., geometry) to get the desired response (e.g., *S*-parameter). This problem is usually solved by an optimization program on a computer, which needs to evaluate the response and possible derivatives with regard to design parameters. This information is obtained from a model, e.g., a circuit model or an EM simulator.

We can consider two kinds of models: "coarse" models (e.g., computationally fast circuit-based model or low-fidelity EM simulation) and "fine" models (e.g., a cpu-intensive full-wave EM simulation). The coarse model (circuit model) is fast to evaluate but inaccurate. The fine model (EM simulation) is accurate but expensive to evaluate.

In order to incorporate the computational efficiency of the (cheap) circuit model and the accuracy of (expensive) EM simulations, Bandler *et al*. introduced

space mapping (SM) technology [1] in 1994. SM-based optimization algorithm performs optimization on the coarse model and calibrates it with the fine model response. This process is similar to the learning process of a designer.

The original algorithm of space mapping [1] was proposed in 1994. In this algorithm, a linear mapping is constructed between coarse and fine parameter spaces.

The aggressive space mapping (ASM) [2][10] technique is developed to exploit each fine model evaluation immediately. A linear mapping between coarse and fine parameter spaces is updated through a Broyden-like update. A quasi-Newton step is used to find satisfactory designs in fine parameter space.

Implicit space mapping (ISM) [7] matches the coarse model with the fine model by calibrating a set of preassigned parameters in the coarse model, e.g., dielectric constant or substrate height.

Output space mapping (OSM) [8][12] matches the coarse model with the fine model by reducing the difference between the coarse and fine model responses.

Artificial neural networks can also be exploited to construct the mapping between coarse and fine parameter spaces to calibrate the coarse model [3]-[5]. A comprehensive review on this topic is given in [6].

Comprehensive reviews on the space mapping technique, including both SM optimization and SM modeling, are given in [9].

In this chapter, we review the ISM and space mapping design framework, which are used in the spiral inductor and LC resonator optimization. We also propose a modified parameter extraction method, which is used in the LC resonator optimization.

3.2 BASIC CONCEPT OF SPACE MAPPING

The basic idea of space mapping is to match the coarse model (typically computationally fast circuit-based model or low-fidelity EM simulation) and the fine model (typically a cpu-intensive full-wave EM simulation) during the optimization, as shown in Fig. 3.1 [9].

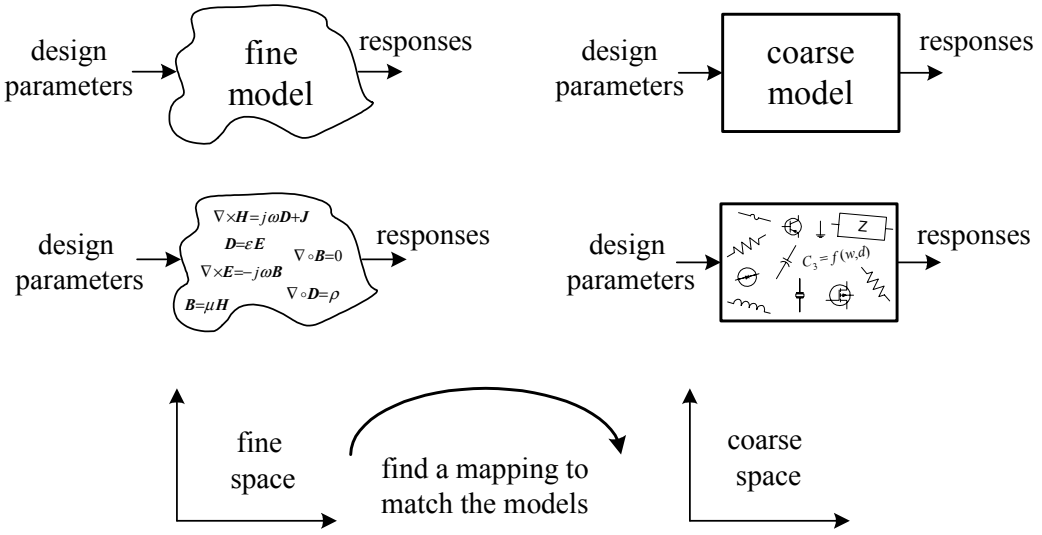

Fig. 3.1 Matching coarse and fine models through a mapping [9].

As shown in Fig. 3.2, we use $\boldsymbol{x}_c \in X_c$ to denote coarse model design parameters and $\boldsymbol{x}_f \in X_f$ to denote fine model design parameters, where $X_c \subseteq \mathbb{R}^{n\times 1}$ and $X_f \subseteq \mathbb{R}^{n\times 1}$ are coarse model and fine model parameter spaces of *n* design parameters. We denote the corresponding vectors of *m* responses (e.g., $|S_{21}|$ at *m* different frequency points) for the coarse model and fine model as $\boldsymbol{R}_c \subseteq \mathbb{R}^{m\times 1}$ and $\boldsymbol{R}_f \subseteq \mathbb{R}^{m\times 1}$, respectively.

The original design problem is to find

$$\boldsymbol{x}_f^* \triangleq \arg\min_{\boldsymbol{x}_f} U(\boldsymbol{R}_f(\boldsymbol{x}_f)) \tag{3.1}$$

where *U* is an objective function of the response, e.g., minimax objective function with upper and lower specification, and $\boldsymbol{x}_f^*$ is the optimal design.

The original idea behind space mapping is to find a mapping between the fine model and coarse model parameter spaces

$$\boldsymbol{x}_c = \boldsymbol{P}(\boldsymbol{x}_f) \tag{3.2}$$

such that

$$\boldsymbol{R}_c(\boldsymbol{P}(\boldsymbol{x}_f)) \approx \boldsymbol{R}_f(\boldsymbol{x}_f) \tag{3.3}$$

in the region of interest.

With this mapping, we can make an estimation of $\boldsymbol{x}_f^*$ without the optimization of the find model

$$\bar{\boldsymbol{x}}_f \triangleq \boldsymbol{P}^{-1}(\boldsymbol{x}_c^*) \tag{3.4}$$

where $\boldsymbol{x}_c^*$ is the coarse model optimal solution.

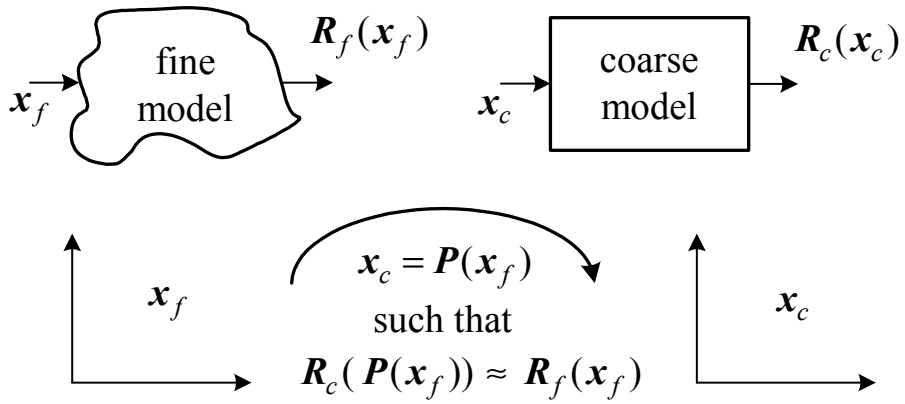

Fig. 3.2 Space mapping notation [9].

3.3 IMPLICIT SPACE MAPPING [7]

Implicit space mapping (ISM) [7] calibrates preassigned parameters, e.g., the dielectric constant and substrate height, through parameter extraction (PE) to match the coarse and fine models. The calibrated model (the surrogate) is reoptimized and the result is used for the fine model evaluation, which provides information for the parameter extraction (calibration) in the next iteration.

As in [7], we define the fine model response at a point $\boldsymbol{x}_f$ in the design space by $\boldsymbol{R}_f(\boldsymbol{x}_f)$ and the coarse-model based surrogate response at a point $\boldsymbol{x}_c$ by $\boldsymbol{R}_c(\boldsymbol{x}_c, \boldsymbol{x}_p)$, where $\boldsymbol{x}_p$ is a set of preassigned parameters. ISM algorithm

involves iterations of two steps [7][11]: ISM modeling through parameter extraction and ISM prediction through surrogate optimization.

ISM modeling adjusts the selected preassigned parameters to match the surrogate with the fine model. As in [7], we denote $\boldsymbol{x}_c^{*(i)}$ as the surrogate optimal point at the *i*th iteration and $\boldsymbol{x}_c^{*(0)}$ as the initial point. ISM modeling at the *i*th iteration is to find

$$\boldsymbol{x}_p^{(i)} \triangleq \arg\min_{\boldsymbol{x}_p} \left\| \boldsymbol{R}_f(\boldsymbol{x}_c^{*(i-1)}) - \boldsymbol{R}_c(\boldsymbol{x}_c^{*(i-1)}, \boldsymbol{x}_p) \right\|. \tag{3.5}$$

ISM modeling can also use multi-point parameter extraction, e.g., exploit all the responses obtained in the previous iterations

$$\boldsymbol{x}_p^{(i)} \triangleq \arg\min_{\boldsymbol{x}_p} \left\| \begin{bmatrix} \boldsymbol{e}_0^T & \boldsymbol{e}_1^T & \cdots & \boldsymbol{e}_{i-1}^T \end{bmatrix}^T \right\| \tag{3.6}$$

where

$$\boldsymbol{e}_j^T = \boldsymbol{R}_f(\boldsymbol{x}_c^{*(j)}) - \boldsymbol{R}_c(\boldsymbol{x}_c^{*(j)}, \boldsymbol{x}_p),\ j = 0, \cdots, i-1. \tag{3.7}$$

After ISM modeling, we optimize the (re)calibrated coarse model (surrogate model) in ISM prediction, i.e., we find

$$\boldsymbol{x}_c^{*(i)} \triangleq \arg\min_{\boldsymbol{x}_c \in X_c} U(\boldsymbol{R}_c(\boldsymbol{x}_c, \boldsymbol{x}_p^{(i)})) \tag{3.8}$$

where X_c is the parameter space of the surrogate model.

This process (ISM modeling and ISM prediction) continues until the stopping criterion is satisfied, e.g., convergence is reached or the specification is met. The basic concept of ISM is illustrated in Fig. 3.3.

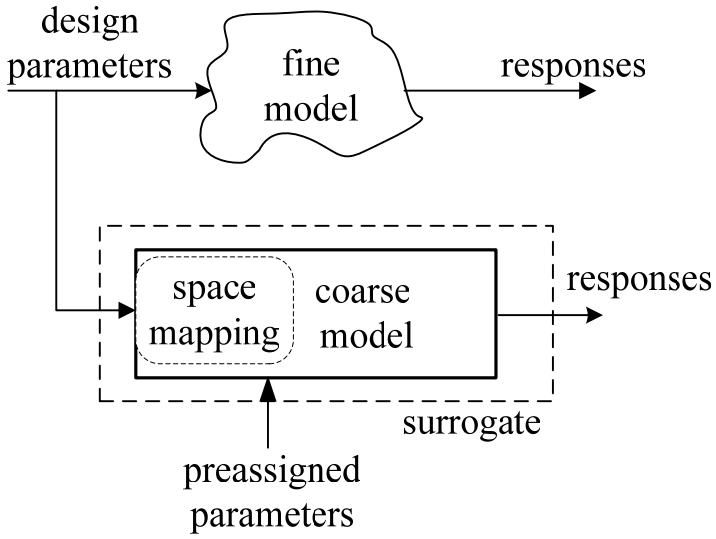

Fig. 3.3 Implicit space mapping concept [7].

3.4 A MODIFIED PARAMETER EXTRACTION SCHEME

Parameter extraction is an important step in ISM. In this section, we propose a modified parameter extraction scheme which is used in the LC resonator optimization.

We denote the vector of component values in the circuit model as $\boldsymbol{x}_{comp} \in \mathbb{R}^{q\times 1}$, where q is the number of component values in the circuit model. For example, we have $\boldsymbol{x}_{comp} = [L_s \; R_s \; C_{ox} \; C_s \; C_{si} \; R_{si}]^T$ for the circuit model of the spiral inductor (Fig. 2.6). In the coarse and surrogate models, $\boldsymbol{x}_{comp}$ is a function of the design parameters $\boldsymbol{x}_c$ and the preassigned parameters $\boldsymbol{x}_p$, e.g., equations for the component values of the spiral inductor given in (2.29) to (2.34). We

denote the corresponding vectors of m responses of the circuit model calculated from $\boldsymbol{x}_{comp}$ as $\boldsymbol{R}_{c,comp} \subseteq \mathbb{R}^{m\times 1}$.

In the ith iteration, we divide the multi-point PE in (3.6) into two separate steps. The first step is to extract the corresponding component values in the circuit model from the fine model responses

$$\boldsymbol{x}_{comp}^{(j)} \triangleq \arg\min_{\boldsymbol{x}_{comp}} \left\| \boldsymbol{R}_f(\boldsymbol{x}_c^{*(j)}) - \boldsymbol{R}_{c,comp}(\boldsymbol{x}_{comp}) \right\|, \; j = 0,\cdots,i-1, \qquad (3.9)$$

where $\boldsymbol{x}_c^{*(j)}$ is the surrogate optimal point in the jth iteration and $\boldsymbol{x}_c^{*(0)}$ is the initial point (coarse model optimum).

The second step is to extract the preassigned parameter from the component values we have obtained

$$\boldsymbol{x}_p^{(i)} \triangleq \arg\min_{\boldsymbol{x}_p} \left\| \begin{bmatrix} \boldsymbol{e}_0^T & \boldsymbol{e}_1^T & \cdots & \boldsymbol{e}_{i-1}^T \end{bmatrix}^T \right\| \qquad (3.10)$$

where

$$\boldsymbol{e}_j^T = \boldsymbol{x}_{comp}^{(j)} - \boldsymbol{x}_{comp}(\boldsymbol{x}_c^{*(j)}, \boldsymbol{x}_p), \; j = 0,\cdots,i-1. \qquad (3.11)$$

The purpose of dividing the PE into two steps is that hopefully one or both of the steps can be turned into convex optimization problems (in the LC resonator optimization problem, the second step is turned into a convex optimization problem as discussed in Appendix A), which can be solved globally and efficiently.

The other modification in the new PE is that at the beginning of the algorithm, we fix some of the preassigned parameters to their initial values and

only extract those preassigned parameters that we consider important. For example, we divide the preassigned parameters into k different groups according to their importance

$$\boldsymbol{x}_p = \left[\boldsymbol{x}_{p,1}^T \; \boldsymbol{x}_{p,2}^T \; \cdots \; \boldsymbol{x}_{p,k}^T \right]^T. \tag{3.12}$$

In the ith ($1 \le i \le k-1$) iteration, instead of extracting all preassigned parameters as in (3.10), we only extract those parameters that are important enough and fix the others to their initial values

$$\begin{aligned} \boldsymbol{x}_p^{(i)} &\triangleq \arg\min_{\boldsymbol{x}_p} \left\| \left[\boldsymbol{e}_0^T \; \boldsymbol{e}_1^T \; \cdots \; \boldsymbol{e}_{i-1}^T \right]^T \right\| \\ s.t.\ \boldsymbol{x}_{p,l} &= \boldsymbol{x}_{p,l}^{(0)},\ l = i+1, i+2, \cdots, k, \end{aligned} \tag{3.13}$$

where $\boldsymbol{x}_{p,l}^{(0)},\ l = i+1, i+2, \cdots, k,$ are the initial values of the preassigned parameters and $\boldsymbol{e}_j^T,\ j = 0, \cdots, i-1,$ are given in (3.11). After the (k–1)th iteration, we start to extract all preassigned parameters as in (3.10).

The purpose of this modification is to ensure that we do not have too many preassigned parameters to extract at the beginning, when we have not obtained enough information for the fine model. It is observed that if we extract too many preassigned parameters from inadequate fine model data, the PE usually gives a surrogate model that is good only at the points used for the extraction, but poor at other points in the design region. This may have a negative effect for the following iterations or even lead to the failure of the algorithm (an example is discussed in Appendix B).

3.5 SPACE MAPPING DESIGN FRAMEWORK [13]

A space mapping design framework is proposed in [13] to implement the original, aggressive, implicit and output space mapping through widely available software. Generally, the SM-based optimization comprises the following steps [9].

Step 1 Fine-model simulation (verification) (typically Agilent Momentum, HFSS, and Sonnet ***em***).

Step 2 Extraction of the parameters of a coarse or surrogate model (typically ADS, MATLAB, and OSA90).

Step 3 Updating the surrogate (typically ADS, MATLAB, and OSA90).

Step 4 (Re)optimization of the surrogate (typically ADS, MATLAB, and OSA90).

A more detailed flowchart of SM based optimization is shown in Fig. 3.4.

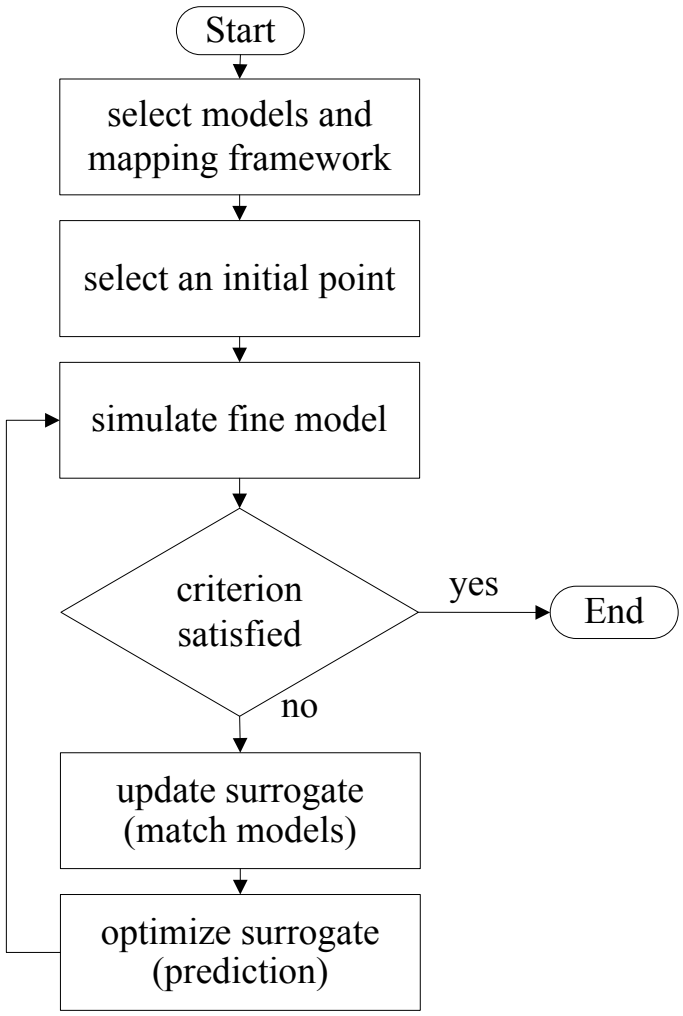

Fig. 3.4 Flowchart of SM-based optimization [13].

REFERENCES

[1] J.W. Bandler, R.M. Biernacki, S.H. Chen, P.A. Grobelny and R.H. Hemmers, "Space mapping technique for electromagnetic optimization," *IEEE Trans. Microwave Theory Tech.*, vol. 42, no. 12, pp. 2536-2544, Dec. 1994.

[2] J.W. Bandler, R.M. Biernacki, S.H. Chen, R.H. Hemmers and K. Madsen, "Electromagnetic optimization exploiting aggressive space mapping," *IEEE Trans. Microwave Theory Tech*., vol. 43, no. 12, pp. 2874-2882, Dec. 1995.

[3] J.W. Bandler, M.A. Ismail, J.E. Rayas-Sánchez and Q.J. Zhang, "Neuromodeling of microwave circuits exploiting space mapping technology," *IEEE Trans. Microwave Theory Tech.*, vol. 47, no. 12, pp. 2417-2427, Dec. 1999.

[4] M.H. Bakr, J.W. Bandler, M.A. Ismail, J.E. Rayas-Sánchez and Q.J. Zhang, "Neural space-mapping optimization for EM-based design," *IEEE Trans. Microwave Theory Tech.*, vol. 48, no. 12, pp. 2307-2315, Dec. 2000.

[5] J.W. Bandler, M.A. Ismail, J.E. Rayas-Sánchez and Q.J. Zhang, "Neural inverse space mapping (NISM) optimization for EM-based microwave design," *Int. J. RF and Microwave CAE*, vol. 13, no. 2, pp. 136-147, Feb. 2003.

[6] J.E. Rayas-Sánchez, "EM-Based optimization of microwave circuits using artificial neural networks: the state-of-the-art," *IEEE Trans. Microwave Theory Tech.*, vol. 52, no. 1, pp. 420-435, Jan. 2004.

[7] J.W. Bandler, Q.S. Cheng, N.K. Nikolova and M.A. Ismail, "Implicit space mapping optimization exploiting preassigned parameters," *IEEE Trans. Microwave Theory Tech.*, vol. 52, no. 1, pp. 378-385, Jan. 2004.

[8] J.W. Bandler, Q.S. Cheng, D. Gebre-Mariam, K. Madsen, F. Pedersen and J. Søndergaard, "EM-based surrogate modeling and design exploiting implicit, frequency and output space mappings," in *IEEE MTT-S Int. Microwave Symp. Dig.,* Philadelphia, PA, 2003, pp. 1003-1006.

[9] J.W. Bandler, Q. Cheng, S.A. Dakroury, A.S. Mohamed, M.H. Bakr, K. Madsen and J. Søndergaard, "Space mapping: the state of the art," *IEEE Trans. Microwave Theory Tech.*, vol. 52, no. 1, pp. 337-361, Jan. 2004.

[10] M.H. Bakr, J.W. Bandler, N.K. Georgieva and K. Madsen, "A hybrid aggressive space-mapping algorithm for EM optimization," *IEEE Trans. Microwave Theory Tech*., vol. 47, no. 12, pp. 2440-2449, Dec. 1999.

[11] W. Yu and J.W. Bandler, "Optimization of spiral inductor on silicon using space mapping," *IEEE MTT-S Int. Microwave Symp. Dig.*, San Francisco, CA, Jun. 2006, pp. 1085-1088.

[12] S. Koziel, J.W. Bandler and K. Madsen, "Towards a rigorous formulation of the space mapping technique for engineering design," *Proc. Int. Symp. Circuits, Syst. ISCAS,* Kobe, Japan, May 2005, pp. 5605-5608.

[13] J.W. Bandler, Q.S. Cheng, D.M. Hailu and N.K. Nikolova, "A space-mapping design framework," *IEEE Trans. Microwave Theory Tech.*, vol. 52, no. 11, pp. 2601-2610, Nov. 2004.

CHAPTER 3 SPACE MAPPING TECHNOLOGY

CHAPTER 4

OPTIMIZATION OF SPIRAL INDUCTORS AND LC RESONATORS USING SPACE MAPPING

4.1 INTRODUCTION

As reviewed in Chapter 2, many methods have been proposed recently to optimize spiral inductors and RF circuits with spiral inductors, including exhaustive enumeration, geometric programming (GP) [1][2], sequential quadratic programming (SQP) [3], Mesh-Adaptive Direct Search (MADS) [4] and so on. These optimization methods are usually based on circuit models of spiral inductors, thus their results depend on the quality of the circuit model they use.

On the other hand, EM solvers, such as Sonnet ***em*** [6] and ADS Momentum [7], provide more accurate models for spiral inductors. However, full-wave EM simulation is so expensive in time that the direct optimization is usually impractical, if not impossible. Besides, some EM solvers require the

structure to be on a grid (e.g., Sonnet ***em*** [6]), which makes it difficult for optimizers to obtain accurate gradients.

In order to incorporate the computational efficiency of (cheap) circuit models and the accuracy of (expensive) EM simulations, we apply the space mapping technique to the optimization of spiral inductors and LC resonators.

We introduce the geometric programming formulation of the spiral inductor optimization proposed in [1] into an implicit space mapping optimization framework. A satisfactory EM-validated spiral inductor design emerges in ten minutes. An exhaustive enumeration based on EM simulation, which takes several days, shows that the fine model optimal solution is obtained with our technique.

The same techniques (implicit space mapping and geometric programming) are extended to the optimization of an LC resonator, in which the inductor is implemented as a spiral inductor. An improved GP formulation of the LC resonator optimization is proposed and a new parameter extraction scheme in ISM algorithm is implemented. An in-house user-friendly software engine for SM-based optimization is also tested. Results show satisfactory EM-validated LC resonator designs can be obtained in approximately ten full-wave simulations.

4.2 A NEW GP FORMULATION OF THE SPIRAL INDUCTOR OPTIMIZATION

As discussed in Section 2.6, the quality factor Q given in (2.22) cannot be directly written into a posynomial function of the design parameters. In [1], a new design variable Q_{min} and a posynomial inequality constraint are introduced.

In [2], a different approach is used. By noticing that $[(\omega L_s / R_s)^2 + 1]R_s$ is much smaller than R_p in the denominator of (2.22), the quality factor is approximated by [2]

$$Q \approx \frac{\omega L_s}{R_s} - \omega R_s (C_s + C_p) - \frac{\omega^3 L_s^2 (C_s + C_p)}{R_s}. \tag{4.1}$$

Equation (4.1) is still not a posynomial function of the design parameters. Although it can be solved using the algorithm mentioned in [2], it is not compatible with standard geometric programming and cannot be solved by commercial optimization software such as MOSEK [5].

We further develop the above approach proposed in [2]. It is noticed that maximizing Q is equivalent to minimizing $1/Q$ and the second and the third term in (4.1) is much smaller than the first term. With a first-order Taylor series approximation, $1/Q$ can be approximated

$$\frac{1}{Q} \approx \frac{R_s}{\omega \cdot L_s}\left[1 + \omega \cdot R_s \cdot (C_s + C_p) \cdot \frac{R_s}{\omega \cdot L_s} + \frac{\omega^3 \cdot L_s^2 \cdot (C_s + C_p)}{R_s} \cdot \frac{R_s}{\omega \cdot L_s}\right]. \tag{4.2}$$

By substituting (2.29) to (2.34) into (4.2), we can write $1/Q$ as a posynomial function of the design parameters

$$\begin{aligned}\frac{1}{Q} &= \frac{k_1 f(\omega)}{\omega\beta} d_{out}^{-\alpha_1} w^{-\alpha_2-1} d_{avg}^{-\alpha_3+1} n^{-\alpha_4+1} s^{-\alpha_5} \\ &+ \frac{k_1^3 f^3(\omega) k_7}{\omega\beta^2} d_{out}^{-2\alpha_1} w^{-2\alpha_2-2} d_{avg}^{-2\alpha_3+4} n^{-2\alpha_4+4} s^{-2\alpha_5} \\ &+ \frac{k_1^3 f^3(\omega) k_3}{\omega\beta^2} d_{out}^{-2\alpha_1} w^{-2\alpha_2-1} d_{avg}^{-2\alpha_3+3} n^{-2\alpha_4+4} s^{-2\alpha_5} \\ &+ \omega k_1 f(\omega) k_7 n^2 d_{avg}^2 + \omega k_1 f(\omega) k_3 n^2 d_{avg} w\end{aligned} \tag{4.3}$$

where k_1, k_3, k_7 and $f(\omega)$ are coefficients dependent on frequency and technology. Equation (4.3) is GP compatible.

4.3 SM-BASED OPTIMIZATION FOR SPIRAL INDUCTORS

We apply the implicit space mapping (ISM) to the spiral inductor optimization problem.

We use Sonnet ***em*** [6] as the fine model. A Matlab [12] driver is developed to generate spiral inductor layout file with the required geometry (d_{out}, w, n and s), as shown in Fig. 4.1. This driver also calls Sonnet ***em*** [6] to simulate the layout file and retrieve the response. We define $\boldsymbol{R}_f = [1/Q_f \;\; L_{sf}]^T$ as the response of the fine model, where [9]

$$Q_f = -\frac{\mathrm{Im}(Y_{11})}{\mathrm{Re}(Y_{11})} \tag{4.4}$$

$$L_{sf} = -\frac{1}{2\pi f}\,\mathrm{Im}\left(\frac{1}{Y_{12}}\right). \tag{4.5}$$

In (4.4) and (4.5), Q_f and L_{sf} are the quality factor and the inductance calculated from the Y parameters obtained from the EM simulation. f is the frequency.

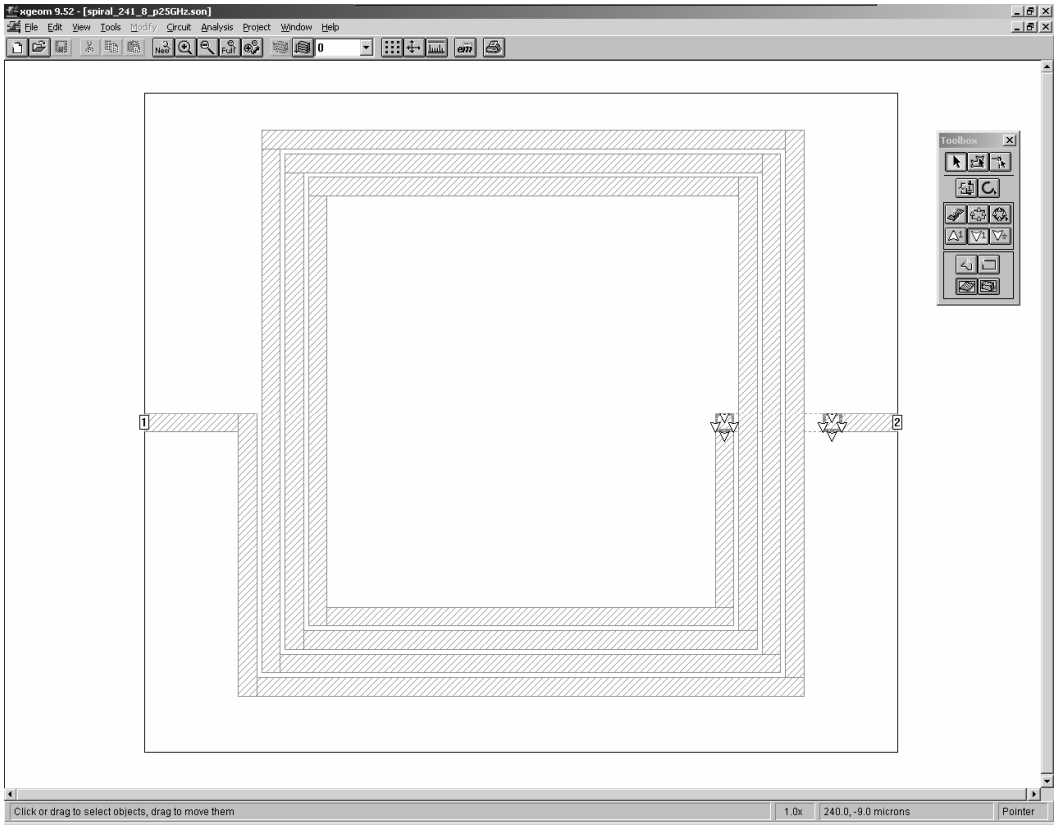

Fig. 4.1 A 3.5 turn spiral inductor layout generated by the Matlab driver for Sonnet ***em***.

The coarse model we use is based on the GP-compatible model [1][8], which is reviewed in Section 2.2 to Section 2.4. We define $\boldsymbol{R}_c = [1/Q_c \;\; L_{sc}]^T$ as the response of the coarse model, where

$$\begin{aligned}\frac{1}{Q_c} &= \frac{k_1}{\omega\beta} d_{out}^{-\alpha_{Q1}} w^{-\alpha_{Q2}-1} d_{avg}^{-\alpha_{Q3}+1} n^{-\alpha_{Q4}+1} s^{-\alpha_{Q5}} \\ &+ \frac{k_1^3 k_7}{\omega\beta^2} d_{out}^{-2\alpha_{Q1}} w^{-2\alpha_{Q2}-2} d_{avg}^{-2\alpha_{Q3}+4} n^{-2\alpha_{Q4}+4} s^{-2\alpha_{Q5}} \\ &+ \frac{k_1^3 k_3}{\omega\beta^2} d_{out}^{-2\alpha_{Q1}} w^{-2\alpha_{Q2}-1} d_{avg}^{-2\alpha_{Q3}+3} n^{-2\alpha_{Q4}+4} s^{-2\alpha_{Q5}} \\ &+ \omega k_1 k_7 n^2 d_{avg}^2 + \omega k_1 k_3 n^2 d_{avg} w\end{aligned} \tag{4.6}$$

$$L_{sc} = \beta d_{out}^{\alpha_{Ls}1} w^{\alpha_{Ls}2} d_{avg}^{\alpha_{Ls}3} n^{\alpha_{Ls}4} s^{\alpha_{Ls}5} . \tag{4.7}$$

Compared with (4.3) and (2.29), two different sets of coefficients, α_{Qi} and α_{Lsi}, i=1, 2, …, 5, are used for $1/Q_c$ and L_{sc} in (4.6) and (4.7). They are the same in the coarse model (surrogate without calibration), but in the surrogate model, they will be treated as different preassigned parameters and extracted separately to calibrate the quality factor and the inductance.

The new GP formulation of the problem (Section 4.2) is used in surrogate optimization. The final GP formulation is

$$\begin{aligned}&\min\ 1/Q_c \\ &s.t.\ L_{s\min} \le \beta d_{out}^{\alpha_{Ls}1} w^{\alpha_{Ls}2} d_{avg}^{\alpha_{Ls}3} n^{\alpha_{Ls}4} s^{\alpha_{Ls}5} \le L_{s\max} \\ &\quad d_{avg} + ns + nw \le d_{out} \\ &\quad (2n+1)(s+w) \le d_{out} \\ &\quad d_{out\min} \le d_{out} \le d_{out\max} \\ &\quad w_{\min} \le w \le w_{\max} \\ &\quad s_{\min} \le s \le s_{\max} \\ &\quad n_{\min} \le n \le n_{\max}\end{aligned} \tag{4.8}$$

where $1/Q_c$ is given in (4.6).

We solve (4.8) with the "mskgpopt" function in the MOSEK optimization toolbox [5]. One problem in solving (4.8) is that the number of turns n should be discrete in a practical design. We address this problem by first considering n as continuous and solving (4.8) to get the optimal n^*. Then we round n^* to the two nearest discrete values n_1^* and n_2^*. Fixing n to n_1^* and n_2^*, we perform another two optimizations. Finally, we choose the better result of these two optimizations as the solution of (4.8).

Implicit space mapping is used in this problem. We define β, α_{Lsi}, k_1, k_3, k_7 and α_{Qi}, $i = 1, 2, \cdots, 5$, as preassigned parameters

$$\boldsymbol{x}_p = [\beta \ \alpha_{Ls1} \ \cdots \ \alpha_{Ls5} \ k_1 \ k_3 \ k_7 \ \alpha_{Q1} \ \cdots \ \alpha_{Q5}]^T. \tag{4.9}$$

The ISM-based optimization algorithm can be summarized as follows [10].

Step 1 Set *j*=0 and pick an initial design parameter $\boldsymbol{x}_c^{*(0)}$.

Step 2 Simulate the fine model at $\boldsymbol{x}_c^{*(j)}$ and increment *j*.

Step 3 Extract the preassigned parameters $\boldsymbol{x}_p^{*(j)}$ by solving (3.6) (ISM modeling).

Step 4 Optimize the (re)calibrated coarse model (surrogate model) to obtain $\boldsymbol{x}_c^{*(j)}$ by solving (4.8).

Step 5 Terminate if a stopping criterion (e.g., convergence) is satisfied.

Step 6 Go to Step 2.

In Step 3, we extract the coefficients for L_s and the coefficients for Q separately. The PE for L_s can be turned into a quadratic programming and solved globally and efficiently (Appendix A). The PE for Q is solved with the "fmincon" function in Matlab [12]. The constraints used in the PE are discussed in Appendix B.

4.4 A SPIRAL INDUCTOR DESIGN EXAMPLE [10]

We apply ISM to optimizing the spiral inductor built with the sample CMOS process shown in Fig. 2.2. The conductivity of the Si substrate is 5 S/m. Two metal layers of 1 μm thickness, M1 and M2, are used for the spiral inductor and the underpass. The conductivity of the metal layers are 3×10^7 S/m.

The specification is to achieve the highest quality factor Q and 4 nH inductance at 3 GHz. The tolerance for the inductance is 5%, which means that the L_s should range from 3.8 nH to 4.2 nH. The constraints on the design parameters are listed in Table 4.1. The number of turns n is restricted to discrete values as k+0.5, where k is a positive integer.

TABLE 4.1

CONSTRAINTS ON THE DESIGN PARAMETERS [10]

Parameter	Minimum Value	Maximum Value
d_{out}	150 μm	300 μm
w	1 μm	15 μm
n	2.5	7.5
s	2 μm	10 μm

We consider the ISM algorithm converges when the distance between the optimal designs in two consecutive iterations gets less than one ($\left\| \boldsymbol{x}_c^{*(i)} - \boldsymbol{x}_c^{*(i-1)} \right\| \le 1$). The initial point is selected as $\boldsymbol{x}_c^{*(0)} = [230\ 8\ 5.5\ 2]^T$ ($\boldsymbol{x}_c = [d_{out}\ w\ n\ s]^T$). The result of the ISM-base optimization is shown in Table 4.2, with the results of circuit-model-based geometric programming [1] and exhaustive enumeration of the fine model. In enumeration, the sampling steps in the design region are 5 μm for d_{out}, 1 μm for w, one turn for n and 2 μm for s. The Q and L_s shown in the table are all obtained from EM simulations. With the ISM algorithm, a satisfactory design emerges in ten EM simulations. In comparison, the result given by the circuit-model based GP [1] does not meet the specification when validated by the EM simulator. Enumeration of the fine model

gives a result very close to that of the ISM algorithm, but takes much longer time (several days).

In Fig. 4.2 we compare the inductance L_s of the coarse model and the surrogate model in the last iteration with the fine model over the design region (n is fixed to 4.5 and s is fixed to 2 μm). It can be seen that the surrogate model is successfully calibrated. A similar result is obtained for the quality factor Q.

TABLE 4.2

COMPARISON OF DIFFERENT METHODS FOR SPIRAL INDUCTOR OPTIMIZATION [10]

Method	Optimal Design ($[d_{out}\ w\ n\ s]^T$ in μm)	Q	L_s (nH)	EM Simulations
ISM	$[203\ 10\ 4.5\ 2]^T$	4.9	3.8	10
Circuit Model GP [1]	$[252\ 15\ 3.5\ 2]^T$	5.2	3.1	0*
Enumeration	$[205\ 10\ 4.5\ 2]^T$	4.9	3.9	13950

* One EM simulation is taken to validate the design. It shows that the specification is not met.

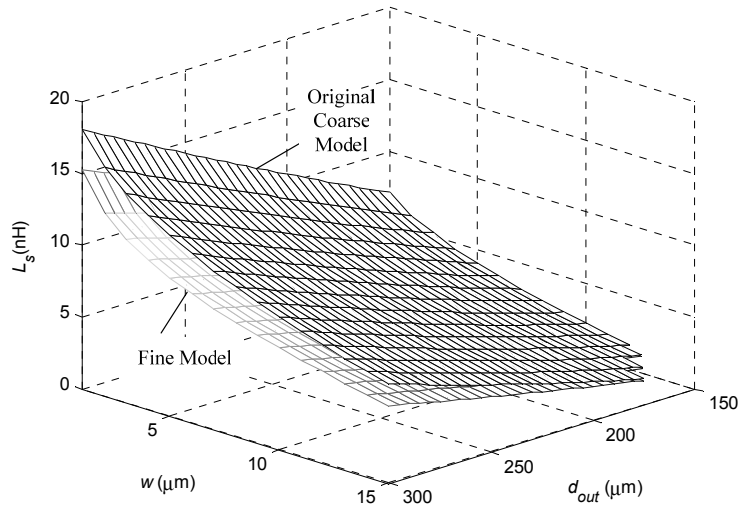

(a)

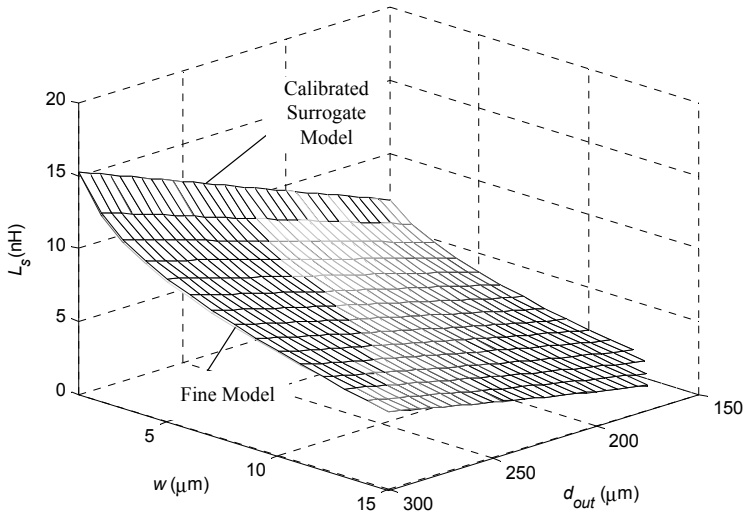

(b)

Fig. 4.2 L_s over the design region (n = 4.5, s = 2 μm): (a) the original coarse and fine models, (b) the calibrated surrogate model in the last iteration and the fine model [10].

4.5 A GP FORMULATION OF LC RESONATOR OPTIMIZATION [1]

The LC resonator (LC tank) is widely used as the load in tuned amplifiers to provide gain at selective frequencies, as shown in Fig. 4.3. In RF ICs, the inductor in the LC resonator is usually implemented as an on-chip spiral inductor.

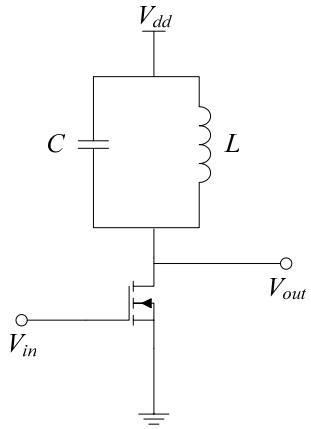

Fig. 4.3 A simple tuned amplifier with the LC resonator as the load [1].

The specification of the LC resonator includes the resonance frequency, the resonant tank impedance and the quality factor. Higher tank impedance leads to higher gain of the tuned amplifier and the higher quality factor leads to narrower bandwidth and better frequency selectivity.

Based on the circuit model of the spiral inductor shown in Fig. 2.6, we can get the circuit model of the LC resonator (Fig. 4.4) by transforming C_{ox}, R_{si} and C_{si}, into its equivalent R_p and C_p, as given by (2.17) and (2.18). In Fig. 4.4, components L_s, R_s, C_s, C_p and R_p forms the equivalent circuit model of the spiral inductor. All of them can be expressed as monomial functions of the geometric

parameters of the spiral inductor. The capacitor C_{load} represents the additional capacitor used in the LC resonator.

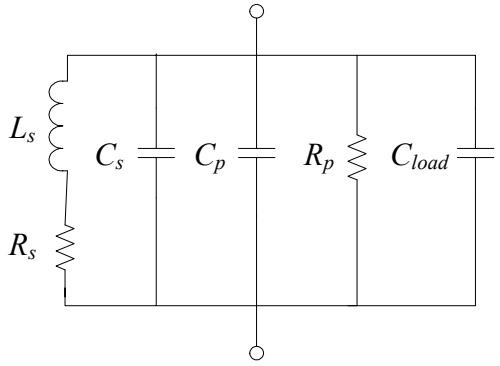

Fig. 4.4 Circuit model of the LC resonator.

The circuit model in Fig. 4.4 can be further simplified into its equivalent circuit shown in Fig. 4.5, in which the components can be expressed as [1]

$$L_{tank} = \left[1 + (R_s / (L_s \omega))^2\right] L_s \tag{4.10}$$

$$C_{tank} = C_{load} + C_s + C_p \tag{4.11}$$

$$R_{tank} = \left(1/R_p + 1/R_{s,p}\right)^{-1} \tag{4.12}$$

where $R_{s,p}$ is the parallel equivalent of R_s, which is given by [1]

$$R_{s,p} = \left[1 + (L_s \omega / R_s)^2\right] R_s \approx (L_s \omega)^2 / R_s . \tag{4.13}$$

The quality factor and resonance frequency of the LC resonator can be calculated as [1]

$$Q_{tank} = R_{tank} / (\omega_{res} L_{tank}) \tag{4.14}$$

$$\omega_{res} = \frac{1}{\sqrt{L_{tank} C_{tank}}} . \tag{4.15}$$

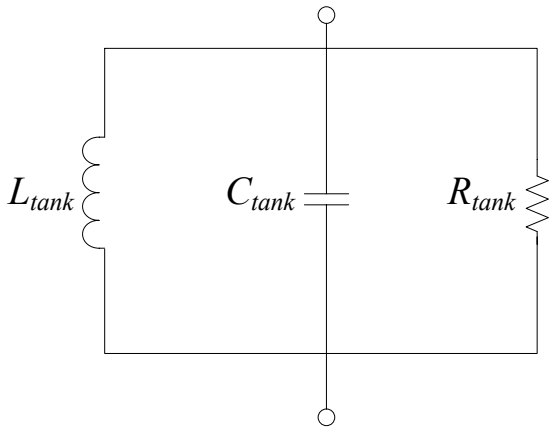

Fig. 4.5 Equivalent circuit model of the LC resonator.

The LC resonator optimization problem can be expressed as [1]

$$\begin{aligned} &\min \ 1/R_{tank} \\ &s.t. \ L_{tank}C_{tank} \le 1/\omega_{res}^2 \\ &\quad Q_{tank} \ge Q_{tank,min} \\ &\quad C_{load} \le C_{load,max} \end{aligned} . \tag{4.16}$$

The design parameters are the geometry parameters of the spiral inductor (d_{out}, w, n, s) and the additional capacitor C_{load}.

As can be seen in (4.12), the objective function $1/R_{tank}$ can be expressed as a posynomial function of the design parameters. The first inequality constraint is for the resonance frequency. It is relaxed from the equality constraint because this constraint is always tight if there is no constraint on the inductor area [1]. Since both L_{tank} and C_{tank} can be expressed as posynomial functions of the design parameters, the relaxed constraint is GP compatible. Also, since both L_{tank} and $1/R_{tank}$ are posynomial functions of the design parameters, the second

constraint on Q_{tank} can be turned into GP compatible form as well. Thus the problem is formulated into a GP.

4.6 AN IMPROVED GP FORMULATION OF LC RESONATOR OPTIMIZATION

As pointed out before, the first constraint in (4.16) is tight only if there is no constraint on inductor area, which will be a limitation in many applications where area constraints are needed. To address this problem, we propose a new GP formulation based on the original one proposed in [1]. We noticed that both Q_{tank} and R_{tank} are only related to the geometry parameters of the spiral inductor (d_{out}, w, n, s), not to the additional capacitor C_{load}. So we divide the problem into two steps. In the first step, we optimize only the geometry parameters of the spiral inductor (d_{out}, w, n, s)

$$\begin{aligned} \min\ & 1/R_{tank} \\ s.t.\ & L_{tank}(C_{load,min}+C_s+C_p) \le 1/\omega_{res}^2 \\ & 1/\omega_{res}^2 \le L_{tank}(C_{load,max}+C_s+C_p) \\ & 1/Q_{tank} \le 1/Q_{tank,min} \end{aligned} \tag{4.17}$$

where the first and the second constraints are to ensure that there exists a C_{load} to achieve the resonance frequency specified. However, the second constraint is not GP compatible. To solve that problem, we notice that usually $C_{load,max}$ is usually much larger than C_s and C_p, and L_{tank} is approximately L_s for practical quality factor ($Q_{tank} > 1.5$). Thus (4.17) is approximately equivalent to

$$\begin{aligned} \min\ & 1/R_{tank} \\ s.t.\ & L_{tank}(C_{load,min} + C_s + C_p) \le 1/\omega_{res}^2 \\ & 1/(L_s C_{load,max}) \le \omega_{res}^2 \\ & 1/Q_{tank} \le 1/Q_{tank,min} \end{aligned} \tag{4.18}$$

which is a GP problem.

In the second step, we calculate C_{load} from the specification of the resonance frequency

$$L_{tank}(C_{load} + C_s + C_p) = 1/\omega_{res}^2 \tag{4.19}$$

where C_s, C_p and L_{tank} are calculated from the geometry parameters of the spiral inductor obtained in the first step.

4.7 SM-BASED OPTIMIZATION FOR LC RESONATOR

We apply the implicit space mapping technique to the optimization of the LC resonator.

The fine model of the LC resonator is the combination of a Sonnet ***em*** model for the spiral inductor and an ideal circuit model for the additional capacitor, as shown in Fig. 4.6. The layout and the responses of the spiral inductor are generated and retrieved by the Matlab driver (see Section 4.3). We define $\boldsymbol{R}_f = [\boldsymbol{Y}_{11f,sp}^T \ \boldsymbol{Y}_{12f,sp}^T]^T$ as the fine model response, where $\boldsymbol{Y}_{11f,sp}$ and $\boldsymbol{Y}_{12f,sp}$ are the Y parameters of the spiral inductor over a range of frequency obtained from EM simulations.

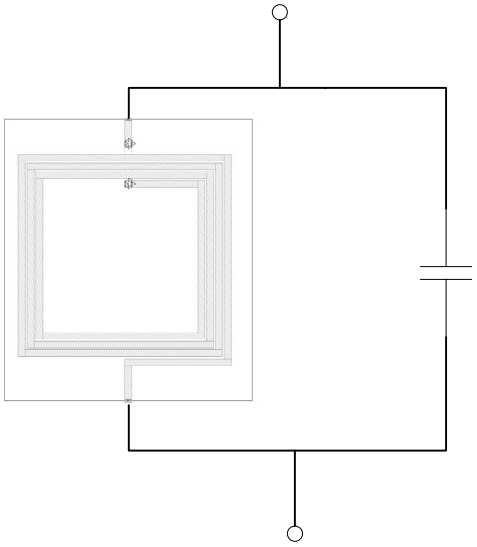

Fig. 4.6 The fine model of the LC resonator.

The coarse model of the resonator is shown in Fig. 4.7. We define $\boldsymbol{R}_c = [\boldsymbol{Y}_{11c,sp}^T \ \boldsymbol{Y}_{12c,sp}^T]^T$ as the coarse model response, where $\boldsymbol{Y}_{11c,sp}$ and $\boldsymbol{Y}_{12c,sp}$ are the *Y* parameters calculated from the coarse model of the spiral inductor (Fig. 4.7 with C_{load} removed), in which the components are calculated as

$$L_s = \beta d_{out}^{\alpha_{Ls1}} w^{\alpha_{Ls2}} d_{avg}^{\alpha_{Ls3}} n^{\alpha_{Ls4}} s^{\alpha_{Ls5}} \tag{4.20}$$

$$R_s = 4k_1 w^{\alpha_{Rs1}} d_{avg}^{\alpha_{Rs2}} n^{\alpha_{Rs3}} f(\omega) \tag{4.21}$$

$$C_{ox} = 4k_2 w^{\alpha_{Cox1}} d_{avg}^{\alpha_{Cox2}} n^{\alpha_{Cox3}} \tag{4.22}$$

$$C_s = k_3 w^{\alpha_{Cs1}} n^{\alpha_{Cs2}} \tag{4.23}$$

$$C_{si} = 4k_4 w^{\alpha_{Cox1}} d_{avg}^{\alpha_{Cox2}} n^{\alpha_{Cox3}} \tag{4.24}$$

$$R_{si} = \frac{k_5}{4} w^{-\alpha_{Cox1}} d_{avg}^{-\alpha_{Cox2}} n^{-\alpha_{Cox3}} . \tag{4.25}$$

Compared with (2.29) to (2.34), (4.20) to (4.25) are more general. In the coarse model, the coefficients in (4.20) to (4.25) are set to the nominal values, which reduce the expressions to (2.29) to (2.34). For example, we set $\alpha_{R_{s1}} = -1$, $\alpha_{R_{s2}} = 1$ and $\alpha_{R_{s3}} = 1$ in the expression of R_s. In the surrogate model, we treat these parameters as preassigned parameters (implicit SM parameters) and calibrate them in the SM optimization process.

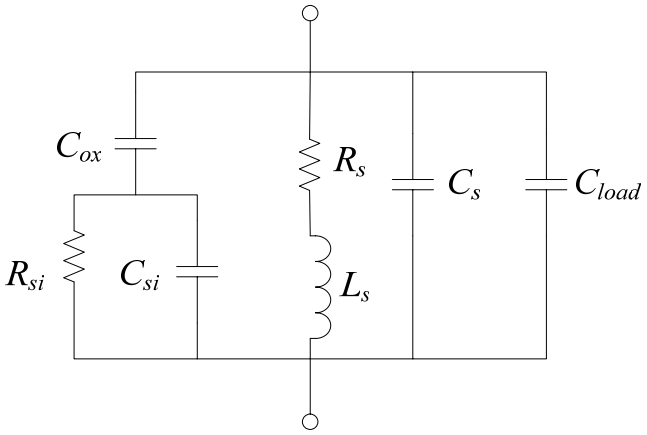

Fig. 4.7 The coarse (surrogate) model of the LC resonator.

Note that in (4.20) to (4.25), we use the same power coefficients ($\alpha_{C_{ox1}}$, $\alpha_{C_{ox2}}$ and $\alpha_{C_{ox3}}$) for C_{ox} and C_{si}, and negative values ($-\alpha_{C_{ox1}}$, $-\alpha_{C_{ox2}}$ and $-\alpha_{C_{ox3}}$) for R_{si} to maintain the compatibility with GP in the surrogate optimization. In the GP formulation of the problem, C_p has to be a posynomial function of the design parameters. This criterion can only be met when the power coefficients for C_{ox}, C_{si} and R_{si} cancel out in the denominator of (2.18).

The surrogate optimization is solved as a GP (Section 4.6) with the MOSEK optimization toolbox [5]. The following parameters are selected as preassigned parameters (implicit SM parameters)

$$\boldsymbol{x}_p = [\beta\ \alpha_{L_s1}\ \alpha_{L_s2}\ k_1\ \alpha_{R_s1}\ \alpha_{R_s2}\ k_2\ \alpha_{C_{ox}1}\ \alpha_{C_{ox}2}\ k_3\ \alpha_{C_s1}\ k_4\ k_5]^T . \quad (4.26)$$

The modified parameter extraction scheme discussed in Section 3.4 is used in this problem. As the first step, we extract the component values in the circuit model from the fine model responses. To do that in the *i*th iteration, we first calculate $\boldsymbol{Y}_{1f,sp}$ and $\boldsymbol{Y}_{2f,sp}$ shown in Fig. 4.8 as

$$\boldsymbol{Y}_{1f,sp}^{(i)} = \boldsymbol{Y}_{11f,sp}^{(i)} + \boldsymbol{Y}_{12f,sp}^{(i)} \quad (4.27)$$

$$\boldsymbol{Y}_{2f,sp}^{(i)} = -\boldsymbol{Y}_{12f,sp}^{(i)} \quad (4.28)$$

where $\boldsymbol{Y}_{11f,sp}^{(i)}$ and $\boldsymbol{Y}_{12f,sp}^{(i)}$ are the vectors of the *Y* parameter obtained in the EM simulation of the spiral inductor in the *i*th iteration.

Then we extract circuit component values from $\boldsymbol{Y}_{1f,sp}^{(i)}$ and $\boldsymbol{Y}_{2f,sp}^{(i)}$

$$\begin{bmatrix} R_{si}^{(i)} & C_{si}^{(i)} & C_{ox}^{(i)} \end{bmatrix} = \arg \min_{R_{si},\, C_{si},\, C_{ox}} \sum_{k=1}^{p} \left\| \frac{(\frac{1}{R_{si}} + j\omega_k C_{si})\, j\omega_k C_{ox}}{\frac{1}{R_{si}} + j\omega_k C_{si} + j\omega_k C_{ox}} - Y_{1f,sp,k}^{(i)} \right\| \quad (4.29)$$

$$\begin{bmatrix} C_s^{(i)} & L_s^{(i)} & k_{R_s}^{(i)} \end{bmatrix} = \arg \min_{C_s,\, L_s,\, k_{R_s}} \sum_{k=1}^{p} \left\| j\omega_k C_s + \frac{1}{j\omega_k L_s + k_{R_s} f(\omega_k)} - Y_{2f,sp,k}^{(i)} \right\| \quad (4.30)$$

where p is the number of the frequencies in the frequency sweep and k_{R_s} is the frequency-independent component of R_s

$$k_{R_s} = 4k_1 w^{\alpha_{R_{s1}}} d_{avg}^{\alpha_{R_{s2}}} n^{\alpha_{R_{s3}}} . \tag{4.31}$$

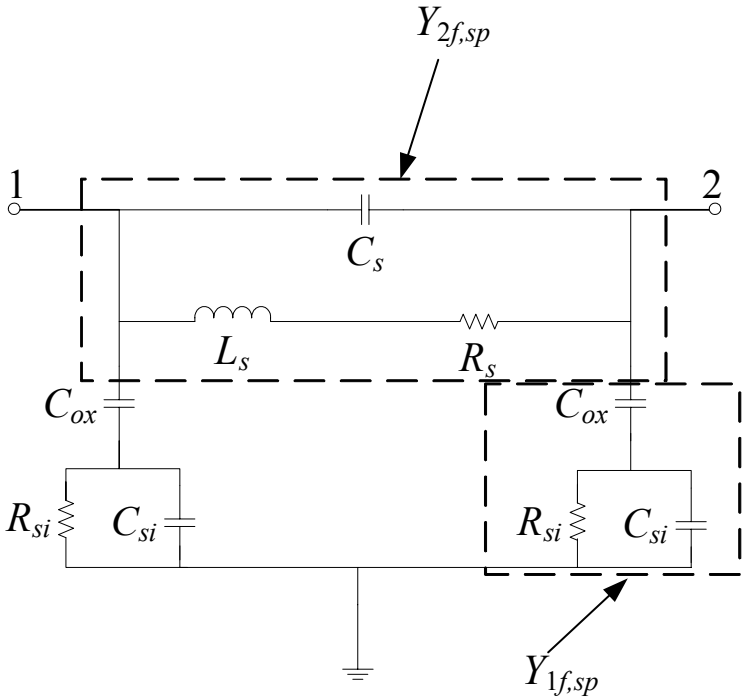

Fig. 4.8 Y_1 and Y_2 in the coarse model of the spiral inductor.

The second step of the modified parameter extraction is to extract the preassigned parameters from the component values $R_{si}^{(k)}$, $C_{si}^{(k)}$, $C_{ox}^{(k)}$, $C_s^{(k)}$, $L_s^{(k)}$ and $k_{R_s}^{(k)}$, $k = 1, \cdots, i$. Since all the component values are monomial functions of the design parameters, this step can be turned into six separate convex problems and solved globally and efficiently (Appendix B).

As discussed in Section 3.4, we divide the preassigned parameters into three groups

$$\boldsymbol{x}_{p,1} = [\beta \; k_1 \; k_2 \; k_3 \; k_4 \; k_5]^T \tag{4.32}$$

$$\boldsymbol{x}_{p,2} = \left[\alpha_{L_s 1} \; \alpha_{R_s 1} \; \alpha_{C_{ox} 1} \; \alpha_{C_s 1}\right]^T \tag{4.33}$$

$$\boldsymbol{x}_{p,3} = \left[\alpha_{L_s 2} \; \alpha_{R_s 2} \; \alpha_{C_{ox} 2}\right]^T . \tag{4.34}$$

In the first iteration, we only extract $\boldsymbol{x}_{p,1}$ and keep the other parameters at their initial (nominal) values. In the second iteration, we only extract $\boldsymbol{x}_{p,1}$ and $\boldsymbol{x}_{p,2}$. After the second iteration, we extract all the parameters. In this way, we avoid extracting too many preassigned parameters at the beginning, when we have not obtained enough information about the fine model. On the other hand, by adding more preassigned parameters at a late stage, we are given more freedom to calibrate the surrogate model so that it can match the fine model better.

The design flow for ISM-based optimization of the LC resonator is the same as that of the spiral inductor (Section 4.3).

4.8 AN LC RESONATOR OPTIMIZATION EXAMPLE

We apply the ISM-based algorithm to the optimization of the LC resonator. The spiral inductor is built with the same CMOS process given in Section 4.4. The additional capacitor in the LC resonator is modeled as an ideal capacitor.

The goal of the optimization is to maximize the tank impedance at the resonance frequency, which is 5 GHz. The 3dB bandwidth of the LC resonator is required to be less than 1.2 GHz. The specification of bandwidth can be turned into the specification of quality factor using the relationship between bandwidth and quality factor $Q_{tank} = \Delta f / f_0$, where Δf is the 3dB bandwidth and f_0 is the center frequency. The equivalent specification on quality factor is that $Q_{tank} \geq 4.17$.

The constraints on the design parameters are listed in Table 4.2. In this example, the design parameters are the outer diameter d_{out} (in μm), the metal width w (in μm) and the capacitance C_{load} (in pF). The number of turns n is fixed to 3.5 turns and the turn spacing s is fixed to be 2 μm. The frequency sweep is from 1 GHz to 10 GHz with the 1 GHz frequency step. The initial point is selected as $\boldsymbol{x}_c^{*(0)} = [200\ 10\ 0.5]^T$, where $\boldsymbol{x}_c = [d_{out}\ w\ C_{load}]^T$.

TABLE 4.3

CONSTRAINTS ON THE DESIGN PARAMETERS

Parameter	Minimum Value	Maximum Value
d_{out}	150 μm	300 μm
w	1 μm	15 μm
C_{load}	0.01 pF	10 pF
n	3.5	3.5
s	2 μm	2 μm

The selection of the preassigned parameters is given in (4.26). The surrogate optimization is solved as a geometric programming problem as discussed in Section 4.6. We consider the ISM algorithm converges when the distance between the optimal designs in two consecutive iterations is less than one ($\left\| \boldsymbol{x}_c^{*(i)} - \boldsymbol{x}_c^{*(i-1)} \right\| \le 1$).

The result of the ISM-based optimization is compared with that of the direct optimization of the coarse model in Fig. 4.9 and Table 4.4. The tank impedance in Fig. 4.9, the 3-dB bandwidth and the resonance frequency in Table 4.4 are all obtained from EM simulations.

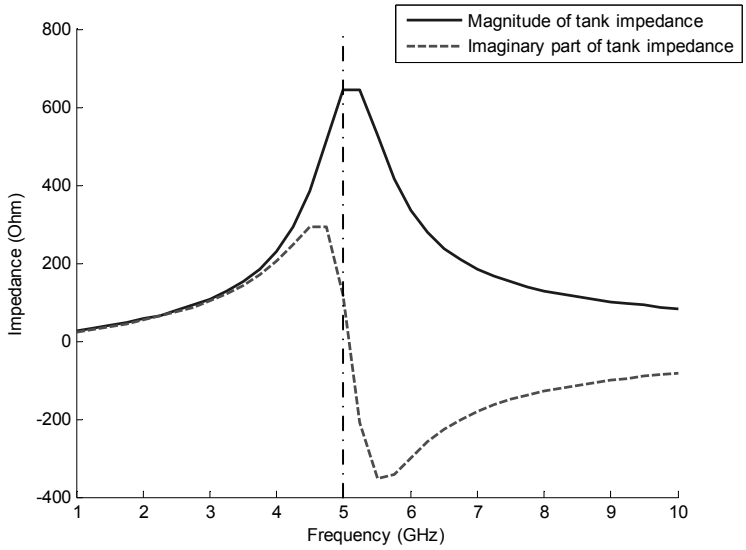

(a)

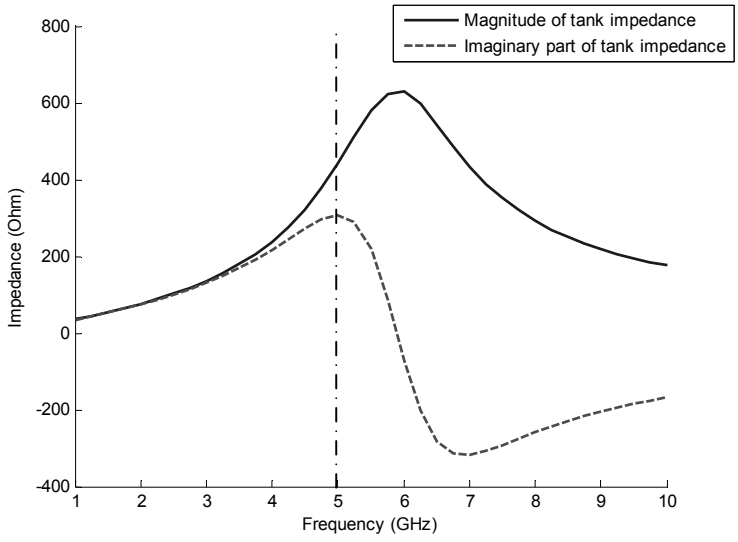

(b)

Fig. 4.9 Tank impedance of the optimal design of the LC resonator given by: (a) ISM, (b) direct optimization of the coarse model. The dashed line at 5 GHz shows the specification of the resonance frequency.

TABLE 4.4

COMPARISON OF DIFFERENT OPTIMIZATION METHODS FOR THE LC RESONATOR OPTIMIZATION

Method	Optimal Design ($[d_{out}\ w\ C_{load}]^T$ in μm and pF)	3-dB Bandwidth (GHz)	Resonance Frequency (GHz)	EM Simulations
ISM	$[216\ 8\ 0.2105]^T$	1.0	5.1	6
Coarse Model Optimization	$[300\ 10\ 0.0591]^T$	1.9	5.9	0*

* One EM simulation is taken to validate the design. It shows that the specification is not met.

It can be seen that within six iterations, the ISM-based optimization algorithm converges to a better design than that given by the direct optimization of the coarse model (when checked with Sonnet ***em***). Compared with the design given by the direct optimization of the coarse model, the design given by ISM-based optimization has the resonance frequency that is closer to the specification (5 GHz) and the 3-dB bandwidth that satisfies the specification (1.2 GHz).

As an alternative, we solve the same problem using the SMF system [11], a prototype user-friendly software package for space mapping optimization. The fine and coarse models are shown in Fig. 4.6 and Fig. 4.7. The frequency sweep is from 3.8 GHz to 6.2 GHz with the 0.3 GHz frequency step. The initial point is selected as $\boldsymbol{x}_c^{*(0)} = [200\ 10\ 1]^T$, where $\boldsymbol{x}_c = [d_{out}\ w\ C_{load}]^T$. The specification is turned into the following minimax specification

$$\begin{aligned} \left\|Z_{tank}\right\| &\geq 700\ \Omega \quad \text{at 5 GHz} \\ \left\|Z_{tank}\right\| &\leq 490\Omega \quad \text{from 3.8 GHz to 4.4 GHz} \\ \left\|Z_{tank}\right\| &\leq 490\Omega \quad \text{from 5.6 GHz to 6.2 GHz} \end{aligned} \tag{4.35}$$

where Z_{tank} is the tank impedance of the LC resonator. The constraints are the same as that shown in Table 4.3.

The minimax optimization engine of Matlab [12] is used for the surrogate optimization. Implicit space mapping is used in this problem with the following preassigned parameters

$$\boldsymbol{x}_p = [\beta\ k_1\ k_2\ k_3\ k_4\ k_5]^T. \tag{4.36}$$

As shown in Fig. 4.10, the specification is met in ten iterations and the design obtained is $\boldsymbol{x}_c^{*(10)} = [234\ 6\ 0.1679]^T$. The LC tank resonates at 5 GHz and has 726 ohms resonance tank impedance.

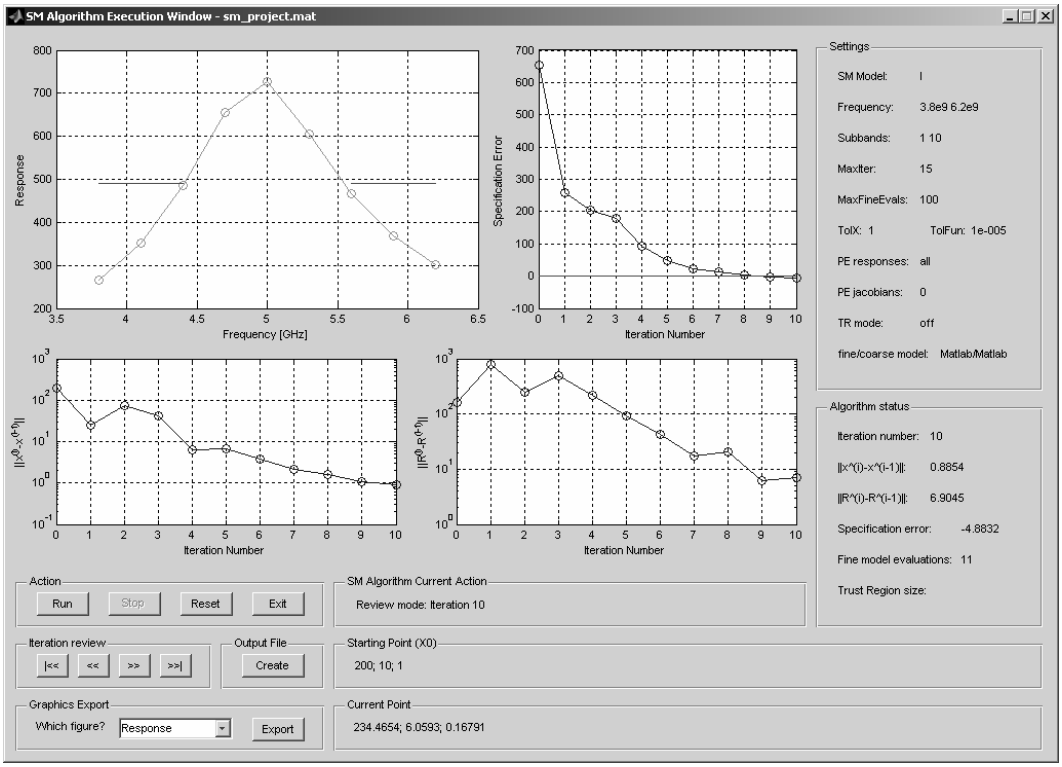

Fig. 4.10 Results obtained in SMF (the graph in the upper-left corner is the final fine model response, the graph in the upper-right corner is the specification error versus iteration number, and the two graphs below is $\left\| \boldsymbol{x}_c^{*(i)} - \boldsymbol{x}_c^{*(i-1)} \right\|$ and $\left\| \boldsymbol{R}_f^{*(i)} - \boldsymbol{R}_f^{*(i-1)} \right\|$ versus the iteration number).

REFERENCES

[1] M. Hershenson, S.S. Mohan, S.P. Boyd and T.H. Lee, "Optimization of inductor circuits via geometric programming," *Proc. 36th Design Automation Conf.*, pp. 994-998, Jun. 1999.

[2] G. Stojanovic and L. Zivanov, "Comparison of optimal design of different spiral inductors," *24th Int. Conf. Microelectronics*, vol. 2, pp. 613-616, May 2004.

[3] Y. Zhan and S.S. Sapatnekar, "Optimization of integrated spiral inductors using sequential quadratic programming," *2004 Design, Automation and Test in Europe Conf. Exhibition*, vol. 1, pp. 622-627, Feb. 2004.

[4] A. Nieuwoudt and Y. Massoud, "Multi-level approach for integrated spiral inductor optimization," *Proc. 42nd Design Automation Conf.*, pp. 648-651, Jun. 2005.

[5] The MOSEK optimization toolbox for MATLAB version 3.2 (Revision 8), MOSEK ApS, c/o Symbion Science Park, Fruebjergvej 3, Box 16, 2100 Copenhagen Ø, Denmark.

[6] ***em***, Sonnet Software, Inc. 100 Elwood Davis Road, North Syracuse, NY 13212, USA.

[7] Agilent Momentum, Agilent Technologies, 1400 Fountaingrove Parkway, Santa Rosa, CA 95403-1799, USA.

[8] S.S. Mohan, M. Hershenson, S.P. Boyd and T.H. Lee, "Simple accurate expressions for planar spiral inductances," *IEEE J. Solid-State Circuits*, vol. 34, no. 10, pp. 1419-1424, Oct. 1999.

[9] K. Okada, H. Hoshino and H. Onodera, "Modeling and optimization of on-chip spiral inductor in S-parameter domain," *2004 Int. Symp. Circuits and Systems*, vol. 5, pp. 153-156, May 2004.

[10] W. Yu and J.W. Bandler, "Optimization of spiral inductor on silicon using space mapping," *IEEE MTT-S Int. Microwave Symp. Dig.*, San Francisco, CA, Jun. 2006, pp.1085-1088.

[11] SMF, Bandler Corporation, P.O. Box 8083, Dundas, ON, Canada L9H 5E7, 2006.

[12] Matlab Version 7.0(2004), The MathWorks, Inc., 3 Apple Hill Drive, Natick, MA 01760-2098.

CHAPTER 5

CONCLUSIONS

In this thesis, we apply the space mapping (SM) technique to the optimization of spiral inductors and LC resonators. With our method, EM-validated designs for spiral inductors and LC resonators usually emerge in ten full-wave EM simulations. Compared with traditional optimization methods, considerable improvement has been obtained.

For the first time, we introduce geometric programming into the space mapping design process, so that the global optimal solution in the surrogate optimization can be ensured. We simplify the GP formulation for spiral inductor optimization and improve the GP formulation for LC resonator optimization.

We propose a modified parameter extraction scheme. By dividing the problem into two steps, we partially transform the parameter extraction in the LC resonator optimization into convex optimization problems, which can be solved globally and efficiently. We propose to use fewer preassigned parameters at the beginning and gradually add preassigned parameters in later iterations. We also discuss the effect of constraints in the parameter extraction.

CHAPTER 5 CONCLUSIONS

In Chapter 2, we reviewed recent work on the modeling and optimization of spiral inductors, including a physically based circuit model, a GP-compatible circuit model and the GP formulation of the spiral inductor optimization problem. We also review the methods for inductance and quality factor calculation.

In Chapter 3, we reviewed the implicit space mapping technique and the general steps for SM-based optimization. We also propose a modified parameter extraction scheme.

In Chapter 4, we present an ISM-based optimization algorithm for spiral inductor design, in which geometric programming is introduced. The same technique is applied to LC resonator design. Two examples show that EM-validated designs of spiral inductors and LC resonators can be obtained in ten full-wave EM simulations.

The author suggests the following future research topics.

(1) Apply our technique to the optimization of other RF circuits with spiral inductors, such as voltage-controlled oscillators (VCO) and low noise amplifiers (LNA).

(2) Apply our technique to the optimization of spiral inductors of other shapes, multi-layer spiral inductors and spiral inductors with patterned ground shields (PGS).

(3) Formulate the parameter extraction into a convex optimization problem.

APPENDIX A

PARAMETER EXTRACTION FOR MONOMIAL FUNCTIONS

As pointed out in [1], the parameter extraction for monomial functions can be turned into a convex optimization problem.

We take the extraction of the coefficients of L_{sc} as an example. The inductance L_{sc} is a function of d_{out}, w, d_{avg}, n and s, as given in (4.7). Suppose in the ith iteration, we have calculated or extracted i different inductance values $L_{sf}^{(k)}, k = 1,\ 2,\ \cdots, i,$ from the fine model responses in the previous iterations. The corresponding geometric parameters (the surrogate optimal solutions) are $d_{out}^{(k)}$, $w^{(k)}$, $d_{avg}^{(k)}$, $n^{(k)}$ and $s^{(k)}, k = 1,\ 2,\ \cdots, i$. To extract β, $\alpha_{L_s 1}$, $\alpha_{L_s 2}$, $\alpha_{L_s 3}$, $\alpha_{L_s 4}$ and $\alpha_{L_s 5}$, we first take the logarithm of both sides of (4.7) and we get

$$\begin{aligned} \log L_{sc} = \log \beta + \alpha_{L_s 1} \log d_{out} + \alpha_{L_s 2} \log w + \\ \alpha_{L_s 3} \log d_{avg} + \alpha_{L_s 4} \log n + \alpha_{L_s 5} \log s \end{aligned} . \tag{A.1}$$

Then the PE process can be turned into the following linear data fitting problem

$$\left[\log\beta \;\; \alpha_{L_s 1} \;\; \alpha_{L_s 2} \;\; \alpha_{L_s 3} \;\; \alpha_{L_s 4} \;\; \alpha_{L_s 5}\right]^T = \arg\min_{\boldsymbol{x}} \left\|\boldsymbol{A}\boldsymbol{x} - \boldsymbol{b}\right\| \tag{A.2}$$

where

$$\boldsymbol{A} = \begin{bmatrix} 1 & \log d_{out}^{(1)} & \log w^{(1)} & \log d_{avg}^{(1)} & \log n^{(1)} & \log s^{(1)} \\ 1 & \log d_{out}^{(2)} & \log w^{(2)} & \log d_{avg}^{(2)} & \log n^{(2)} & \log s^{(2)} \\ \vdots & \vdots & \vdots & \vdots & \vdots & \vdots \\ 1 & \log d_{out}^{(i)} & \log w^{(i)} & \log d_{avg}^{(i)} & \log n^{(i)} & \log s^{(i)} \end{bmatrix} \tag{A.3}$$

$$\boldsymbol{b} = \begin{bmatrix} \log L_{sf}^{(1)} \\ \log L_{sf}^{(2)} \\ \vdots \\ \log L_{sf}^{(i)} \end{bmatrix}. \tag{A.4}$$

If we use the l_2 norm in (A.2), the problem can be turned into the following quadratic programming problem

$$\begin{aligned} &\left[\log\beta \;\; \alpha_{L_s 1} \;\; \alpha_{L_s 2} \;\; \alpha_{L_s 3} \;\; \alpha_{L_s 4} \;\; \alpha_{L_s 5}\right]^T \\ &= \arg\min_{\boldsymbol{x}} \; (\boldsymbol{x}^T \boldsymbol{A}^T \boldsymbol{A}\boldsymbol{x} - 2\boldsymbol{b}^T \boldsymbol{A}\boldsymbol{x} + \boldsymbol{b}^T \boldsymbol{b}) \end{aligned} \tag{A.5}$$

which can be solved with the "quadprog" function in Matlab [2] or the "mskqpopt" function in MOSEK [3].

REFERENCES

[1] S.S. Mohan, M. Hershenson, S.P. Boyd and T.H. Lee, "Simple accurate expressions for planar spiral inductances," *IEEE J. Solid-State Circuits*, vol. 34, no. 10, pp. 1419-1424, Oct. 1999.

[2] Matlab Version 7.0(2004), The MathWorks, Inc., 3 Apple Hill Drive, Natick, MA 01760-2098.

[3] The MOSEK optimization toolbox for MATLAB version 3.2 (Revision 8), MOSEK ApS, c/o Symbion Science Park, Fruebjergvej 3, Box 16, 2100 Copenhagen Ø, Denmark.

APPENDIX A PARAMETER EXTRACTION FOR MONOMIAL FUNCTIONS

APPENDIX B

CONSTRAINTS IN PARAMETER EXTRACTION FOR SPIRAL INDUCTOR OPTIMIZATION

We denote the elements of the preassigned parameter vector $\boldsymbol{x}_p$ as $x_{p,k}$, $k = 1,\ 2,\ \cdots, l$. In the optimization of spiral inductors, we use following constraints in the parameter extraction of the *i*th iteration

$$x_{plb,k}^{(i)} \le x_{p,k} \le x_{pub,k}^{(i)},\ k = 1,\ 2,\ \cdots, l, \tag{B.1}$$

where

$$x_{plb,k}^{(i)} = \begin{cases} (1-r)^i x_{p,k}^{(0)} & \text{for } x_{p,k}^{(0)} \ge 0 \\ (1+r)^i x_{p,k}^{(0)} & \text{for } x_{p,k}^{(0)} < 0 \end{cases} \tag{B.2}$$
$$k = 1,\ 2,\ \cdots, l,$$

$$x_{pub,k}^{(i)} = \begin{cases} (1+r)^i x_{p,k}^{(0)} & \text{for } x_{p,k}^{(0)} \ge 0 \\ (1-r)^i x_{p,k}^{(0)} & \text{for } x_{p,k}^{(0)} < 0 \end{cases} \tag{B.3}$$
$$k = 1,\ 2,\ \cdots, l,$$

where $x_{p,k}^{(0)}$, $k = 1,\ 2,\ \cdots, l,$ is the element of the initial value (nominal value) of $\boldsymbol{x}_p$. In (B.2) and (B.3), the boundaries for the preassigned parameters extraction

are iteration-dependent. We allow more freedom (larger feasible region for preassigned parameters) as the iteration number increases. The coefficient r ($0 \le r \le 1$) is used to adjust the rate of this freedom increase. We choose r as 0.2 in our spiral inductor optimization example.

The purpose of the above iteration-dependent constraints is to ensure that the surrogate model does not go too far from the coarse model when we have not obtained adequate fine model data to extract the preassigned parameters.

We compared the effect of different constraints in Table B.1. The first two rows are for the fixed (iteration-independent) constraints (the first row for small feasible region and the second row for large feasible region). The last row is for the iteration-dependent constraint discussed above.

It is observed that the solutions obtained with the fixed (iteration-independent) constraints in the first and the second rows are far away from the fine model optimal (we consider the solution $[205\ 10\ 4.5\ 2]^T$ obtained by enumeration as the fine model optimal). The possible reason is that for the constraints in the first row, the feasible region for the preassigned parameters might be too small to allow the surrogate model to be calibrated well enough. For the constraints in the second row, the feasible region for the preassigned parameters may be so big that the surrogate model goes too far from the coarse model in beginning, only matching the fine model at the points used for parameter extraction. This may lead to the failure of the algorithm.

TABLE B.1

COMPARISON OF DIFFERENT CONSTRAINTS FOR SPIRAL INDUCTOR OPTIMIZATION

Constraints	Solution Obtained ($[d_{out}\ w\ n\ s]^T$ in μm)	Number of Iterations*
$x_{plb,k}^{(i)} = \begin{cases} 0.5x_{p,k}^{(0)} & \text{for } x_{p,k}^{(0)} \geq 0 \\ 2x_{p,k}^{(0)} & \text{for } x_{p,k}^{(0)} < 0 \end{cases}$ $x_{pub,k}^{(i)} = \begin{cases} 2x_{p,k}^{(0)} & \text{for } x_{p,k}^{(0)} \geq 0 \\ 0.5x_{p,k}^{(0)} & \text{for } x_{p,k}^{(0)} < 0 \end{cases}$ $k = 1,\ 2,\ \cdots,\ l$	$[287\ 15\ 3.5\ 2]^T$	4
$x_{plb,k}^{(i)} = \begin{cases} 0.1x_{p,k}^{(0)} & \text{for } x_{p,k}^{(0)} \geq 0 \\ 10x_{p,k}^{(0)} & \text{for } x_{p,k}^{(0)} < 0 \end{cases}$ $x_{pub,k}^{(i)} = \begin{cases} 10x_{p,k}^{(0)} & \text{for } x_{p,k}^{(0)} \geq 0 \\ 0.1x_{p,k}^{(0)} & \text{for } x_{p,k}^{(0)} < 0 \end{cases}$ $k = 1,\ 2,\ \cdots,\ l$	$[150\ 1\ 3.5\ 2]^T$	7
$x_{plb,k}^{(i)} = \begin{cases} (1-0.2)^i x_{p,k}^{(0)} & \text{for } x_{p,k}^{(0)} \geq 0 \\ (1+0.2)^i x_{p,k}^{(0)} & \text{for } x_{p,k}^{(0)} < 0 \end{cases}$ $x_{pub,k}^{(i)} = \begin{cases} (1+0.2)^i x_{p,k}^{(0)} & \text{for } x_{p,k}^{(0)} \geq 0 \\ (1-0.2)^i x_{p,k}^{(0)} & \text{for } x_{p,k}^{(0)} < 0 \end{cases}$ $k = 1,\ 2,\ \cdots,\ l$	$[203\ 10\ 4.5\ 2]^T$	10

* We consider that the ISM algorithm converges when the distance between the optimal designs in two consecutive iterations is less than one ($\left\| \boldsymbol{x}_c^{*(i)} - \boldsymbol{x}_c^{*(i-1)} \right\| \leq 1$).

APPENDIX B CONSTRAINTS … FOR SPIRAL INDUCTOR OPTIMIZATION

BIBLIOGRAPHY

A.A. Abidi, "RF CMOS comes of age," *IEEE J. Solid-State Circuits*, vol. 39, no. 4, pp. 549-561, Apr. 2004.

Agilent Momentum, Agilent Technologies, 1400 Fountaingrove Parkway, Santa Rosa, CA 95403-1799, USA.

K.B. Ashby, I.A. Koullias, W.C. Finley, J.J. Bastek and S. Moinian, "High Q inductors for wireless applications in a complementary silicon bipolar process," *IEEE J. Solid-State Circuits*, vol. 31, no. 1, pp. 4-9, Jan. 1996.

M.H. Bakr, J.W. Bandler, M.A. Ismail, J.E. Rayas-Sánchez and Q.J. Zhang, "Neural space-mapping optimization for EM-based design," *IEEE Trans. Microwave Theory Tech.*, vol. 48, no. 12, pp. 2307-2315, Dec. 2000.

M.H. Bakr, J.W. Bandler, N.K. Georgieva and K. Madsen, "A hybrid aggressive space-mapping algorithm for EM optimization," *IEEE Trans. Microwave Theory Tech.*, vol. 47, no. 12, pp. 2440-2449, Dec. 1999.

J.W. Bandler, R.M. Biernacki, S.H. Chen, P.A. Grobelny and R.H. Hemmers, "Space mapping technique for electromagnetic optimization," *IEEE Trans. Microwave Theory Tech.*, vol. 42, no. 12, pp. 2536-2544, Dec. 1994.

J.W. Bandler, R.M. Biernacki, S.H. Chen, R.H. Hemmers and K. Madsen, "Electromagnetic optimization exploiting aggressive space mapping," *IEEE Trans. Microwave Theory Tech.*, vol. 43, no. 12, pp. 2874-2882, Dec. 1995.

J.W. Bandler, Q.S. Cheng, S.A. Dakroury, A.S. Mohamed, M.H. Bakr, K. Madsen and J. Søndergaard, "Space mapping: the state of the art," *IEEE Trans. Microwave Theory and Tech.*, vol. 52, no. 1, pp. 337-361, Jan. 2004.

J.W. Bandler, Q.S. Cheng, S.A. Dakroury, A.S. Mohamed, M.H. Bakr, K. Madsen and J. Søndergaard, "Trends in space mapping technology for

engineering optimization," *3rd Annual McMaster Optimization Conference: Theory and Applications, MOPTA03*, Hamilton, ON, Aug. 2003.

J.W. Bandler, Q.S. Cheng, D. Gebre-Mariam, K. Madsen, F. Pedersen and J. Søndergaard, "EM-based surrogate modeling and design exploiting implicit, frequency and output space mappings," *IEEE MTT-S Int. Microwave Symp. Dig.*, Philadelphia, PA, 2003, pp. 1003-1006.

J.W. Bandler, Q.S. Cheng, D.M. Hailu and N.K. Nikolova, "A space-mapping design framework," *IEEE Trans. Microwave Theory Tech.*, vol. 52, no. 11, pp. 2601-2610, Nov. 2004.

J.W. Bandler, Q.S. Cheng, N.K. Nikolova and M.A. Ismail, "Implicit space mapping optimization exploiting preassigned parameters," *IEEE Trans. Microwave Theory Tech.*, vol. 52, no. 1, pp. 378-385, Jan. 2004.

J.W. Bandler, D.M. Hailu, K. Madsen and F. Pedersen, "A space mapping interpolating surrogate algorithm for highly optimized EM-based design of microwavee devices," *IEEE Trans. Microwave Theory and Tech.*, vol. 52, no. 11, pp. 2593-2600, Nov. 2004.

J.W. Bandler, M.A. Ismail, J.E. Rayas-Sánchez and Q.J. Zhang, "Neural inverse space mapping (NISM) optimization for EM-based microwave design," *Int. J. RF and Microwave CAE*, vol. 13, no. 2, pp. 136-147, Feb. 2003.

J.W. Bandler, M.A. Ismail, J.E. Rayas-Sánchez and Q.J. Zhang, "Neuromodeling of microwave circuits exploiting space mapping technology," *IEEE Trans. Microwave Theory Tech.*, vol. 47, no. 12, pp. 2417-2427, Dec. 1999.

H.G. Booker, *Energy in Electromagnetism*, London/New York: Peter Peregrinus (on behalf of the IEE), 1982.

S. Boyd and L. Vandenberghe, *Convex Optimization*, Cambridge University Press, Cambridge, 2004.

J.N. Burghartz, D.C. Edelstein, M. Soyuer, H.A. Ainspan and K.A. Jenkins, "RF circuit design aspects of spiral inductors on silicon," *IEEE J. Solid-State Circuits*, vol. 33, no. 12, pp. 2028-2034, Dec. 1998.

J.N. Burghartz, M. Soyuer and K. Jenkins, "Microwave inductors and capacitors in standard multilevel interconnect silicon technology," *IEEE Trans. Microwave Theory Tech.*, vol. 44, no. 1, pp. 100-103, Jan. 1996.

J.N. Burghartz, M. Soyuer and K. Jenkins, "Microwave inductors and capacitors in standard multilevel interconnect silicon technology," *IEEE Trans. Microwave Theory Tech.*, vol. 44, no. 1, pp. 100-103, Jan. 1996.

J.Y.-C. Chang, A.A. Abidi and M. Gaitan, "Large suspended inductors on silicon and their use in a 2-μm CMOS RF amplifier," *IEEE Electron Device Lett.*, vol. 14, no. 5, pp. 246-248, May 1993.

em, Sonnet Software, Inc. 100 Elwood Davis Road, North Syracuse, NY 13212, USA.

H.M. Greenhouse, "Design of planar rectangular microelectronic inductors," *IEEE Trans. Parts, Hybrids, Pack.*, vol. 10, no. 2, pp. 101-109, Jun. 1974.

F.W. Grover, *Inductance Calculations*, New York, NY: Van Nostrand, 1962.

M. Hershenson, S.S. Mohan, S.P. Boyd and T.H. Lee, "Optimization of inductor circuits via geometric programming," *Proc. 36th Design Automation Conf.*, pp. 994-998, Jun. 1999.

H. Jiang, Y. Wang, J.L. Andrew and N.C. Tien, "On-chip spiral inductors suspended over deep copper-lined cavities," *IEEE Trans. Microwave Theory Tech.*, vol. 48, no.12, pp. 2415-2423, Dec. 2000.

S. Koziel, J.W. Bandler and K. Madsen, "Towards a rigorous formulation of the space mapping technique for engineering design," *Proc. Int. Symp. Circuits, Syst. ISCAS*, Kobe, Japan, May 2005, pp. 5605-5608.

C.-Y. Lee, T.-S. Chen, J.D.-S. Deng and C.-H. Kao, "A simple systematic spiral inductor design with perfected Q improvement for CMOS RFIC application," *IEEE Trans. Microwave Theory Tech.*, vol. 53, no. 2, pp. 523-528, Feb. 2005.

J.R. Long and M.A. Copeland, "The modeling, characterization, and design of monolithic inductors for silicon RF IC's," *IEEE J. Solid-State Circuits*, vol. 32, no. 3, pp. 357-369, Mar. 1997.

Matlab Version 7.0(2004), The MathWorks, Inc., 3 Apple Hill Drive, Natick, MA 01760-2098, USA.

R.B. Merrill, T.W. Lee, H. You, R. Rasmussen and L.A. Moberly, "Optimization of high Q integrated inductors for multi-level metal CMOS," *IEDM 1995*, pp. 38.7.1-38.7.3.

BIBLIOGRAPHY

S.S. Mohan, M. Hershenson, S.P. Boyd and T.H. Lee, "Simple accurate expressions for planar spiral inductances," *IEEE J. Solid-State Circuits*, vol. 34, no. 10, pp. 1419-1424, Oct. 1999.

N.M. Nguyen and R.G. Meyer, "Si IC-compatible inductors and LC passive filters," *IEEE J. Solid-State Circuits*, vol. 25, no. 4, pp. 1028-1031, Aug. 1990.

A. Nieuwoudt and Y. Massoud, "Multi-level approach for integrated spiral inductor optimization," *Proc. 42nd Design Automation Conf.*, pp. 648-651, Jun. 2005.

A. Niknejad, ASITIC: Analysis and Simulation of Spiral Inductors and Transformers for ICs, Univ. California, Berkeley, [Online]. Available: http://rfic.eecs.berkeley.edu/~niknejad/asitic.html.

K. Okada, H. Hoshino and H. Onodera, "Modeling and optimization of on-chip spiral inductor in S-parameter domain," *2004 Int. Symp. Circuits and Systems*, vol. 5, pp. 153-156, May 2004.

J.Y. Park and M.G. Allen, "High Q spiral-type microinductors on silicon substrates," *IEEE Trans. Magn.*, vol. 35, no. 5, pp. 3544-3546, Sept. 1999.

J.E. Rayas-Sánchez, "EM-Based optimization of microwave circuits using artificial neural networks: the state-of-the-art," *IEEE Trans. Microwave Theory Tech.*, vol. 52, no. 1, pp. 420-435, Jan. 2004.

G.M. Rebeiz, *RF MEMS: Theory, Design and Technology*, New York: Wiley, 2003.

SMF, Bandler Corporation, P.O. Box 8083, Dundas, ON, Canada L9H 5E7, 2006.

G. Stojanovic and L. Zivanov, "Comparison of optimal design of different spiral inductors," *24th Int. Conf. Microelectronics*, vol. 2, pp. 613-616, May 2004.

The MOSEK optimization toolbox for MATLAB version 3.2 (Revision 8), MOSEK ApS, c/o Symbion Science Park, Fruebjergvej 3, Box 16, 2100 Copenhagen Ø, Denmark.

J.B. Yoon, Y.S. Choi, B.I. Kim, Y. Eo and E. Yoon, "CMOS-compatible surface-micromachined suspended-spiral inductors for multi-GHz silicon RF ICs," *IEEE Electron Device Lett.*, vol. 23, no. 10, pp. 591-593, Oct. 2002.

W. Yu and J.W. Bandler, "Optimization of spiral inductor on silicon using space mapping," *IEEE MTT-S Int. Microwave Symp.* Dig., San Francisco, CA, Jun. 2006, pp. 1085-1088.

C.P. Yue, C. Ryu, J. Lau, T.H. Lee and S.S. Wong, "A physical model for planar spiral inductors on silicon," *Techn. Dig. IEDM*, pp. 155-158, 1996.

C. Yue and S. Wong, "On-chip spiral inductors with patterned ground shields for Si-based RF IC's," *IEEE J. Solid State Circuits*, vol. 33, no. 5, pp. 743-752, May 1998.

C.P. Yue and S.S. Wong, "Physical modeling of spiral inductors on silicon," *IEEE Trans. on Electron Devices*, vol. 47, no. 3, pp. 560-568, Mar. 2000.

Y. Zhan and S.S. Sapatnekar, "Optimization of integrated spiral inductors using sequential quadratic programming," *2004 Design, Automation and Test in Europe Conf. Exhibition*, vol. 1, pp. 622-627, Feb. 2004.

BIBLIOGRAPHY

AUTHOR INDEX

A

B

C

D

E

F

G

H

I

J

K

L

M

N

O

P

R

S

AUTHOR INDEX

SUBJECT INDEX

A

C

D

E

F

G

I

L

M

P

Q

R

S